Magnetoexcitons in cuprous oxide

Frank Schweiner, Jörg Main, and Günter Wunner

Institut für Theoretische Physik 1, Universität Stuttgart, 70550 Stuttgart, Germany

Marcel Freitag, Julian Heckötter, Christoph Uihlein, Marc Aßmann, Dietmar Fröhlich, and Manfred Bayer

Experimentelle Physik 2, Technische Universität Dortmund, 44221 Dortmund, Germany

Two of the most striking experimental findings when investigating exciton spectra in cuprous oxide using high-resolution spectroscopy are the observability and the fine structure splitting of F excitons reported by J. Thewes *et al.* [Phys. Rev. Lett. **115**, 027402 (2015)]. These findings show that it is indispensable to account for the complex valence band structure and the cubic symmetry of the solid in the theory of excitons. This is all the more important for magnetoexcitons, where the external magnetic field reduces the symmetry of the system even further. We present the theory of excitons in Cu_2O in an external magnetic field and especially discuss the dependence of the spectra on the direction of the external magnetic field, which cannot be understood from a simple hydrogenlike model. Using high-resolution spectroscopy, we also present the corresponding experimental spectra for cuprous oxide in Faraday configuration. The theoretical results and experimental spectra are in excellent agreement as regards not only the energies but also the relative oscillator strengths. Furthermore, this comparison allows for the determination of the fourth Luttinger parameter κ of this semiconductor.

I. INTRODUCTION

Excitons are of great physical interest since they represent the fundamental optical excitation in semiconductors. Excitons in cuprous oxide (Cu_2O), in particular, have attracted lots of attention in recent years [1–14] due to an experiment, in which the hydrogenlike absorption spectrum of these quasiparticles could be observed up to a principal quantum number of $n = 25$ [1]. The discovery of these giant Rydberg excitons may pave the way to a deeper understanding of interparticle interactions in the solid [1] and to applications in quantum information technology [14].

In this context it is indispensable to completely understand the underlying theory of excitons. Excitons consist of a negatively charged electron in the conduction band and a positively charged hole in the valence band. As the interaction between electron and hole can be described by a screened Coulomb interaction, excitons are often regarded as the solid-state analog of a hydrogen atom [15–18]. However, the hydrogenlike model of excitons is generally too simple to describe exciton spectra correctly. It has recently been shown that even without external fields this model is incapable of describing the fine structure splitting observed experimentally and that it is inevitable to account for the complex valence band structure and the cubic symmetry O_h of Cu_2O in a quantitative theory [6,8].

This is all the more important in the presence of an external magnetic field, which reduces the symmetry of Cu_2O to a lower symmetry. For this reason one expects an extremely complex splitting of exciton lines in absorption spectra, in which also anticrossings appear. Hence earlier theoretical treatments of these spectra using a hydrogenlike model were unable to describe the vast number of lines observed in experiments (see Refs. [19–22] and further references therein). On the other hand, due to the specific material parameters in Cu_2O, the exciton radius a_{exc} is much larger than the Bohr radius a_0 known from atomic physics. This makes excitons attractive for investigations in external fields [5] since the region of

"high magnetic fields" can be reached within several Tesla, in contrast to the hydrogen atom, where this region begins above several hundreds of Tesla [5,20].

We present the theory for the exciton absorption spectra of Cu_2O in an external magnetic field and solve the corresponding Schrödinger equation using a complete basis. This method also allows for the direct calculation of relative oscillator strengths. We especially discuss the dependence of the spectra on the direction of the external magnetic field, which is well described by the anisotropic band structure and which cannot be understood from a simple hydrogenlike model. Using high resolution spectroscopy to study natural crystals, we also present the complex experimental absorption spectra for the $n \leqslant 7$ exciton states in Faraday configuration with a significantly better resolution than in previous work on this topic [19–22]. The comparison of theory and experiment shows an excellent agreement. It furthermore allows for the determination of a yet not precisely determined material parameter of Cu_2O, i.e., the fourth Luttinger parameter κ.

The paper is organized as follows: In Sec. II we present the Hamiltonian of excitons in external fields in the case of degenerate valence bands and the method of solving the Schrödinger equation in a complete basis. We explain how to calculate relative oscillator strengths in Sec. III. In Sec. IV the experimental setup is described and the absorption spectra of excitons in a uniform magnetic field are discussed. In Sec. V we investigate the symmetry of the Hamiltonian and compare theoretical with experimental spectra for different orientations of the magnetic field to determine the fourth Luttinger parameter of Cu_2O. Finally, we give a short summary and outlook in Sec. VI.

II. HAMILTONIAN

In this section we present the theory of exciton spectra of Cu_2O in a uniform magnetic field. The lowest conduction band in Cu_2O is almost parabolic in the vicinity of the Γ point or the

center of the first Brillouin zone. Therefore, the kinetic energy of an electron in this Γ_6^+ conduction band is given by

$$H_e(\boldsymbol{p}_e) = \frac{\boldsymbol{p}_e^2}{2m_e} \tag{1}$$

with the effective electron mass m_e. Since Cu_2O has cubic symmetry, we use the irreducible representations $\Gamma_i^\pm$ of the cubic group O_h to assign the symmetry of the bands. In contrast to the conduction band, the three uppermost valence bands in Cu_2O are nonparabolic but deformed due to interband interactions and the presence of the nonspherical symmetry of the solid. Hence the kinetic energy of the hole is given by the more complex expression [7,8]

$$\begin{aligned}
H_h(\boldsymbol{p}_h) = {} & H_{so} + (1/2\hbar^2 m_0)\big\{\hbar^2(\gamma_1 + 4\gamma_2)\boldsymbol{p}_h^2 \\
& + 2(\eta_1 + 2\eta_2)\boldsymbol{p}_h^2(\boldsymbol{I} \cdot \boldsymbol{S}_h) - 6\gamma_2\big(p_{h1}^2 I_1^2 + \text{c.p.}\big) \\
& - 12\eta_2\big(p_{h1}^2 I_1 S_{h1} + \text{c.p.}\big) \\
& - 12\gamma_3(\{p_{h1}, p_{h2}\}\{I_1, I_2\} + \text{c.p.}) \\
& - 12\eta_3(\{p_{h1}, p_{h2}\}(I_1 S_{h2} + I_2 S_{h1}) + \text{c.p.})\big\}, \tag{2}
\end{aligned}$$

with $\boldsymbol{p} = (p_1, p_2, p_3)$, $\{a,b\} = \frac{1}{2}(ab + ba)$, and c.p. denoting cyclic permutation. The parameters γ_i and m_0 denote the first three Luttinger parameters and the free electron mass, respectively. The parameters η_i are much smaller than the Luttinger parameters [8]. All of these coefficients describe the behavior and the anisotropic effective mass of the hole in the vicinity of the Γ point. The matrices $\boldsymbol{I}_j$ and $\boldsymbol{S}_{hj}$ denote the three spin matrices of the quasispin $I = 1$ and the hole spin $S_h = 1/2$ while $\boldsymbol{I}$ and $\boldsymbol{S}_h$ are vectors containing these matrices, i.e.,

$$\boldsymbol{I} \cdot \boldsymbol{S}_h = \sum_{j=1}^{3} I_j S_{hj}. \tag{3}$$

The quasispin $I = 1$ describes the threefold degenerate valence band and is a convenient abstraction to denote the three orbital Bloch functions xy, yz, and zx [23]. Due to the spin-orbit coupling between the quasispin I and the hole spin S_h [24]

$$H_{so} = \frac{2}{3}\Delta\left(1 + \frac{1}{\hbar^2}\boldsymbol{I} \cdot \boldsymbol{S}_h\right), \tag{4}$$

the sixfold degenerate valence band (including the hole spin) splits into a higher lying twofold-degenerate band of symmetry Γ_7^+ and a lower lying fourfold-degenerate band of symmetry Γ_8^+ by an amount of Δ.

The Hamiltonian of the exciton is then given by [24,25]

$$H = E_g + V(\boldsymbol{r}_e - \boldsymbol{r}_h) + H_e(\boldsymbol{p}_e) + H_h(\boldsymbol{p}_h), \tag{5}$$

with the energy E_g of the band gap and the Coulomb interaction, which is screened by the dielectric constant ε:

$$V(\boldsymbol{r}_e - \boldsymbol{r}_h) = -\frac{e^2}{4\pi\varepsilon_0\varepsilon}\frac{1}{|\boldsymbol{r}_e - \boldsymbol{r}_h|}. \tag{6}$$

The exchange interaction as well as the central-cell corrections described in Refs. [8,26] are not included in the Hamiltonian (5) as they do not affect the exciton states treated in Secs. IV and V.

In the presence of an external magnetic field, the corresponding Hamiltonian is obtained via the minimal substitution. After introducing relative and center of mass coordinates [27,28] and setting the position and momentum of the center of mass to zero, the complete Hamiltonian of the relative motion reads [17,27–32]

$$\begin{aligned}
H = {} & E_g + V(\boldsymbol{r}) + H_B \\
& + H_e(\boldsymbol{p} + e\boldsymbol{A}(\boldsymbol{r})) + H_h(-\boldsymbol{p} + e\boldsymbol{A}(\boldsymbol{r})). \tag{7}
\end{aligned}$$

Since the magnetic field $\boldsymbol{B}$ is constant in our experiments, we use the vector potential $\boldsymbol{A} = (\boldsymbol{B} \times \boldsymbol{r})/2$. The term H_B describes the energy of the spins in the magnetic field [23,30,32,33]:

$$H_B = \mu_B[g_c \boldsymbol{S}_e + (3\kappa + g_s/2)\boldsymbol{I} - g_s \boldsymbol{S}_h] \cdot \boldsymbol{B}/\hbar. \tag{8}$$

Here μ_B denotes the Bohr magneton, $g_s \approx 2$ the g factor of the hole spin S_h, and g_c the g factor of the conduction band or the electron spin S_e. The value of the fourth Luttinger parameter κ is unknown and will be determined in Sec. V. In the case of a finite spin-orbit coupling Δ an additional term would generally appear in H_B, which depends on the fifth Luttinger parameter q [23,32,33]. However, this term is connected with spin-orbit interactions of higher order [32] and is not considered here. All material values used in our calculations are listed in Table I.

For the case that the magnetic field is oriented along one of the directions of high symmetry, i.e., along the [001], [110], or [111] direction, we rotate the coordinate system to make the quantization axis coincide with the direction of the magnetic field and then express the Hamiltonian (7) in terms of irreducible tensors [32,36,37] (see Appendix A). We can then calculate a matrix representation of the Schrödinger equation corresponding to the Hamiltonian (7) using a complete basis.

As regards the angular momentum part of the basis, we have to consider that the different parts of the Hamiltonian couple the quasispin I, the hole spin S_h, and the angular momentum L of the exciton. Due to the spin orbit coupling H_{so} and the cubic part of the Hamiltonian (7), we introduce the effective hole spin $J = I + S_h$ and the angular momentum $F = L + J$. We finally include the electron spin in our basis by introducing the total angular momentum $F_t = F + S_e$. For the radial part of the exciton wave function we use the Coulomb-Sturmian functions [38]

$$U_{NL}(r) = N_{NL}(2\rho)^L e^{-\rho} L_N^{2L+1}(2\rho), \tag{9}$$

TABLE I. Material parameters used in the calculations. Note that the value of γ_1' is a result of the analysis in Sec. V and slightly differs from the value $\gamma_1' = 2.77$ of Ref. [7].

Band gap energy	$E_g = 2.17208$ eV	[1]
Electron mass	$m_e = 0.99 m_0$	[34]
Dielectric constant	$\varepsilon = 7.5$	[35]
Spin-orbit coupling	$\Delta = 0.131$ eV	[7]
Valence band parameters	$\gamma_1' = 2.74$	[7]
	$\mu' = 0.0586$	[7]
	$\delta' = -0.404$	[7]
	$\eta_1 = -0.02$	[7]
	$\nu = 2.167$	[7]
	$\tau = 1.5$	[7]
g factor of cond. band	$g_c = 2.1$	[21]

with $\rho = r/\alpha$, a normalization factor N_{NL}, the associated Laguerre polynomials $L_n^m(x)$, and an arbitrary scaling parameter α. The radial quantum number N is related to the principal quantum number n via $n = N + L + 1$. Finally, we use the following ansatz for the exciton wave function

$$|\Psi\rangle = \sum_{NLJFF_tM_{F_t}} c_{NLJFF_tM_{F_t}}|\Pi\rangle, \tag{10a}$$

$$|\Pi\rangle = |N, L; (I, S_h) J; F, S_e; F_t, M_{F_t}\rangle, \tag{10b}$$

with real coefficients c. The parenthesis and semicolons in Eq. (10b) shall illustrate the coupling scheme of the spins and the angular momenta.

Inserting the ansatz (10) in the Schrödinger equation $H\Psi = E\Psi$ and multiplying from the left with another basis state $\langle\Pi'|$, we obtain a matrix representation of the Schrödinger equation of the form

$$\boldsymbol{D}\boldsymbol{c} = E\boldsymbol{M}\boldsymbol{c}. \tag{11}$$

The vector $\boldsymbol{c}$ contains the coefficients of the ansatz (10). All matrix elements, which enter the symmetric matrices $\boldsymbol{D}$ and $\boldsymbol{M}$ and which have not been treated in Ref. [8], are given in the Appendixes C and D. The generalized eigenvalue problem (11) is finally solved using an appropriate LAPACK routine [39].

III. OSCILLATOR STRENGTHS

With the solutions of the eigenvalue problem (11) one can directly calculate the relative oscillator strengths for the transitions from the ground state of the solid to the exciton states. In doing so, four important points need to be considered [8].

(i) The transition is parity forbidden, for which reason the transition matrix element is proportional to the gradient of the envelope function at $r = 0$ and the exciton state must have a component with angular momentum $L = 1$. (ii) The dipole operator does not change the total spin $S = S_e + S_h = 0$ of the electron and the hole. (iii) The total symmetry of the exciton state must be identical to the symmetry of the dipole operator. (iv) The quasispin I transforms according to Γ_5^+ whereas a normal spin one transforms according to Γ_4^+. Therefore, since $\Gamma_5^+ = \Gamma_2^+ \otimes \Gamma_4^+$ holds for the cubic group [40], one has to multiply all symmetries with Γ_2^+ [6].

The dipole operator transforms according to the irreducible representation D^1 of the full rotation group. Hence it transforms in Cu$_2$O according to the irreducible representation Γ_4^- of the cubic group O_h. Since the coupling of $S = 0$, $L = 1$, and $I = 1$ leads to a total angular momentum of $F_t = 0$, $F_t = 1$, and $F_t = 2$, one has to find in this nine-dimensional space the three correct linear combinations of states, which transform according to Γ_4^-. The reduction of the representations D^{F_t} of the full rotation group with the inclusion of the additional factor Γ_2^+ yields [41]

$$\tilde{D}^0 = D^0 \otimes \Gamma_2^+ = \Gamma_1^- \otimes \Gamma_2^+ = \Gamma_2^-, \tag{12a}$$

$$\tilde{D}^1 = D^1 \otimes \Gamma_2^+ = \Gamma_4^- \otimes \Gamma_2^+ = \Gamma_5^-, \tag{12b}$$

$$\tilde{D}^2 = D^2 \otimes \Gamma_2^+ = (\Gamma_3^- \oplus \Gamma_5^-) \otimes \Gamma_2^+ = \Gamma_3^- \oplus \Gamma_4^-. \tag{12c}$$

We see that Γ_4^- is included only in the reduction of the irreducible representation D^{F_t} with $F_t = 2$. Using the relations

given in Ref. [40], one can finally find the three linear combinations of $F_t = 2$ states, which transform according to Γ_4^- and which are connected to light being linearly polarized in x, y, and z direction:

$$|\pi_x\rangle = \frac{i}{\sqrt{2}}[|2, -1\rangle_D + |2, 1\rangle_D], \tag{13a}$$

$$|\pi_y\rangle = \frac{1}{\sqrt{2}}[|2, -1\rangle_D - |2, 1\rangle_D], \tag{13b}$$

$$|\pi_z\rangle = \frac{i}{\sqrt{2}}[|2, -2\rangle_D - |2, 2\rangle_D]. \tag{13c}$$

Here $|F_t, M_{F_t}\rangle_D$ is a short notation for the state

$$|(S_e, S_h) S, I; I + S, L; F_t, M_{F_t}\rangle$$
$$= |(1/2, 1/2) 0, 1; 1, 1; F_t, M_{F_t}\rangle, \tag{14}$$

in which the coupling scheme of the spins and angular momenta is different from the one of Eq. (10b)

$$S_e + S_h = S \rightarrow (I + S) + L = F_t \tag{15}$$

due to the requirement that S must be a good quantum number.

To determine the relative oscillator strength of an arbitrary exciton state with the wave function Ψ [see Eq. (10)], we have to account for its $|\pi_x\rangle$, $|\pi_y\rangle$, or $|\pi_z\rangle$ component. Hence the relative oscillator strength for light being linearly polarized in x direction is, e.g., given by

$$f_{rel} \sim \left|\lim_{r\to 0} \frac{\partial}{\partial r}\langle\pi_x|\Psi(\boldsymbol{r})\rangle\right|^2, \tag{16}$$

with $r = |\boldsymbol{r}|$ (see also Appendix B). Note that when considering the coupling scheme of the angular momenta and spins in Eq. (10b) there are only three combinations of $L = 1$, J, and F, which lead to a total angular momentum of $F_t = 2$. These are

$$L = 1, \quad J = 1/2 \rightarrow F = 3/2, \tag{17a}$$

$$L = 1, \quad J = 3/2 \rightarrow F = 3/2, \tag{17b}$$

$$L = 1, \quad J = 3/2 \rightarrow F = 5/2. \tag{17c}$$

Hence the oscillator strength is definitely zero if all the coefficients $c_{N1\frac{1}{2}\frac{3}{2}2M_{F_t}}$, $c_{N1\frac{3}{2}\frac{3}{2}2M_{F_t}}$, and $c_{N1\frac{3}{2}\frac{5}{2}2M_{F_t}}$ in the exciton state Ψ are zero [cf. Eq. (10)].

In the presence of an external magnetic field the operator $\boldsymbol{A}_{rad}\boldsymbol{p}$, which describes the interaction between the radiation field or light and the exciton and which enters the dipole matrix element, has to be replaced by $\boldsymbol{A}_{rad}[\boldsymbol{p} + e\boldsymbol{A}(\boldsymbol{r})]$ due to the minimal substitution. However, the second term is generally small in comparison to the first one and it vanishes in the Faraday configuration considered here [42–44].

Nevertheless, we have to consider that the magnetic field reduces the symmetry of the system. Furthermore, since the incident light is oriented parallel to $\boldsymbol{B}$ and since we choose the quantization axis parallel to $\boldsymbol{B}$, we have to find the correct linear combinations of the $F_t = 2$ states, which describe linearly or circularly polarized light for the three orientations of the magnetic field considered here. This will be done in the following.

A. Magnetic field in [001] direction

In a magnetic field, which is oriented along the [001] direction, the symmetry O_h of the system is reduced to C_{4h} and we have to consider the reduction of the irreducible representation Γ_4^- of O_h by the group C_{4h}:

$$\Gamma_4^- \rightarrow \Gamma_1^- \oplus \Gamma_3^- \oplus \Gamma_4^-. \qquad (18)$$

Using the method of projection operators [40], we can determine the correct linear combinations of the states in Eq. (13) which transform according to the irreducible representations of C_{4h}:

$$\Gamma_1^- : |\pi_z\rangle = \frac{i}{\sqrt{2}}[|2,-2\rangle_D - |2,2\rangle_D], \qquad (19a)$$

$$\Gamma_3^- : |\sigma_z^+\rangle = \frac{-i}{\sqrt{2}}[|\pi_x\rangle + i|\pi_y\rangle] = |2,-1\rangle_D, \qquad (19b)$$

$$\Gamma_4^- : |\sigma_z^-\rangle = \frac{i}{\sqrt{2}}[|\pi_x\rangle - i|\pi_y\rangle] = -|2,1\rangle_D. \qquad (19c)$$

One can see that Γ_1^- is connected with light which is linearly polarized along [001], i.e., in the z direction. This light cannot be observed along the z axis due to the Faraday configuration in the experiment. Γ_3^- as well as Γ_4^- are connected with circularly polarized light. Consequently, only states of the symmetry Γ_3^- or Γ_4^- can be observed in absorption experiments and we calculate the relative oscillator strengths by evaluating

$$f_{\text{rel}} \sim \left| \lim_{r \to 0} \frac{\partial}{\partial r} \langle \sigma_z^\pm | \Psi(\boldsymbol{r}) \rangle \right|^2. \qquad (20)$$

Note that the sign of $\sigma^\pm$ is defined by the direction of rotation of the polarization with respect to $\boldsymbol{B}$.

B. Magnetic field in [110] direction

In a magnetic field, which is directed in [110] direction, the symmetry O_h of the system is reduced to C_{2h}. In this case the reduction of the irreducible representation Γ_4^- of O_h by the group C_{4h} reads

$$\Gamma_4^- \rightarrow \Gamma_1^- \oplus \Gamma_2^- \oplus \Gamma_2^- \qquad (21)$$

and the correct linear combinations of the states in Eq. (13) which transform according to the irreducible representations of C_{2h} are

$$\Gamma_1^- : \frac{1}{\sqrt{2}}[|\pi_x\rangle + |\pi_y\rangle], \qquad (22a)$$

$$\Gamma_2^- : |\pi_z\rangle, \qquad (22b)$$

$$\Gamma_2^- : \frac{1}{\sqrt{2}}[|\pi_x\rangle - |\pi_y\rangle]. \qquad (22c)$$

We see that Γ_1^- is connected with light which is linearly polarized along [110] and that Γ_2^- is connected with transverse polarized light in [001] and [1$\bar{1}$0] direction. Since the states $|\pi_x\rangle$ and $|\pi_y\rangle$ transform according to the same irreducible representation, we can also use the following linear combinations, which describe circularly polarized light:

$$\Gamma_2^- : \mp \frac{i}{\sqrt{2}}\left[|\pi_z\rangle \pm \frac{i}{\sqrt{2}}[|\pi_x\rangle - |\pi_y\rangle] \right]. \qquad (23)$$

We now choose the quantization axis parallel to $\boldsymbol{B}$, i.e., we rotate the coordinate system by the Euler angles $(\alpha, \beta, \gamma) = (\pi, \pi/2, \pi/4)$. This coordinate transformation reads

$$\boldsymbol{r}' = \begin{pmatrix} x' \\ y' \\ z' \end{pmatrix} = \frac{1}{\sqrt{2}} \begin{pmatrix} 0 & 0 & \sqrt{2} \\ 1 & -1 & 0 \\ 1 & 1 & 0 \end{pmatrix} \begin{pmatrix} x \\ y \\ z \end{pmatrix} = \boldsymbol{R}\boldsymbol{r}. \qquad (24)$$

Note that the direction of the x' and y' axis are predefined by the crystal axes. Rotating the states of Eq. (22) as well yields

$$\Gamma_1^- : |\pi_{z'}\rangle = \frac{1}{\sqrt{2}}[|2,-1\rangle_D - |2,1\rangle_D], \qquad (25a)$$

$$\Gamma_2^- : |\pi_{x'}\rangle = \frac{\sqrt{3}}{2}|2,0\rangle_D + \frac{1}{\sqrt{8}}[|2,-2\rangle_D + |2,2\rangle_D], \qquad (25b)$$

$$\Gamma_2^- : |\pi_{y'}\rangle = \frac{i}{\sqrt{2}}[|2,2\rangle_D - |2,-2\rangle_D], \qquad (25c)$$

or

$$\Gamma_2^- : |\sigma_{z'}^\pm\rangle = \mp \frac{i}{\sqrt{2}}[|\pi_{x'}\rangle \pm i|\pi_{y'}\rangle]. \qquad (26a)$$

Finally, we calculate the relative oscillator strengths by evaluating

$$f_{\text{rel}} \sim \left| \lim_{r \to 0} \frac{\partial}{\partial r} \langle \pi_{x',y'} | \Psi(\boldsymbol{r}) \rangle \right|^2 \qquad (27)$$

for light which is polarized in [001] or in [1$\bar{1}$0] direction or

$$f_{\text{rel}} \sim \left| \lim_{r \to 0} \frac{\partial}{\partial r} \langle \sigma_{z'}^\pm | \Psi(\boldsymbol{r}) \rangle \right|^2 \qquad (28)$$

for circularly polarized light.

C. Magnetic field in [111] direction

In a magnetic field, which is directed in [111] direction, the symmetry O_h of the system is reduced to C_{3i}. In this case we have

$$\Gamma_4^- \rightarrow \Gamma_1^- \oplus \Gamma_2^- \oplus \Gamma_3^- \qquad (29)$$

and the correct linear combinations of the states in Eq. (13) read

$$\Gamma_1^- : \frac{1}{\sqrt{3}}[|\pi_x\rangle + |\pi_y\rangle + |\pi_z\rangle], \qquad (30a)$$

$$\Gamma_2^- : \frac{-i}{\sqrt{2}}\left[\frac{1}{\sqrt{6}}[|\pi_x\rangle + |\pi_y\rangle - 2|\pi_z\rangle] + i\frac{1}{\sqrt{2}}[-|\pi_x\rangle + |\pi_y\rangle] \right], \qquad (30b)$$

$$\Gamma_3^- : \frac{i}{\sqrt{2}}\left[\frac{1}{\sqrt{6}}[|\pi_x\rangle + |\pi_y\rangle - 2|\pi_z\rangle] - i\frac{1}{\sqrt{2}}[-|\pi_x\rangle + |\pi_y\rangle] \right]. \qquad (30c)$$

We see that Γ_1^- is connected with light which is linearly polarized along [111] and that Γ_2^- and Γ_3^- are connected with circularly polarized light transverse to this axis.

For $\boldsymbol{B} \parallel [111]$ we rotate the coordinate system by the Euler angles $(\alpha, \beta, \gamma) = (0, \arccos(1/\sqrt{3}), \pi/4)$. This coordinate transformation reads

$$\boldsymbol{r}'' = \begin{pmatrix} x'' \\ y'' \\ z'' \end{pmatrix} = \frac{1}{\sqrt{6}} \begin{pmatrix} 1 & 1 & -2 \\ -\sqrt{3} & \sqrt{3} & 0 \\ \sqrt{2} & \sqrt{2} & \sqrt{2} \end{pmatrix} \begin{pmatrix} x \\ y \\ z \end{pmatrix} = \boldsymbol{R}\boldsymbol{r}.$$

(31)

Rotating the states of Eq. (30) yields

$$\Gamma_1^- : \ |\pi_{z''}\rangle = |2, 0\rangle_D,$$

(32a)

$$\Gamma_2^- : \ |\sigma_{z''}^+\rangle = \frac{i}{\sqrt{3}} [\sqrt{2}|2, -2\rangle_D - |2, 1\rangle_D],$$

(32b)

$$\Gamma_3^- : \ |\sigma_{z''}^-\rangle = \frac{-i}{\sqrt{3}} [\sqrt{2}|2, 2\rangle_D + |2, -1\rangle_D],$$

(32c)

and we calculate the relative oscillator strengths by evaluating

$$f_{\text{rel}} \sim \left| \lim_{r \to 0} \frac{\partial}{\partial r} \langle \sigma_{z''}^\pm | \Psi(\boldsymbol{r}) \rangle \right|^2.$$

(33)

IV. EXPERIMENT

In the experiment, we investigated the absorption α of Cu$_2$O crystal slabs that were cut and polished from a natural rock. Three different samples with different orientations were prepared: in the first sample the [001] direction is normal to the crystal surface; in the other two samples the normal direction corresponds to the [110] and [111] orientation, respectively. The thicknesses of these samples varied from 30 to 50 μm which is, however, of no relevance for the results described below. For application of a magnetic field, the samples were inserted in a superconducting split coil magnet with a helium cryostat in the center, in which the samples were cooled down to $T = 1.4$ K. The magnetic field direction was chosen to be along the optical axis (Faraday configuration), i.e., also normal to the studied crystal slabs.

The absorption was measured using a white light source which was filtered by a double monochromator such that only the energy range in which the exciton states of interest are located was covered. The exciting light was circularly polarized by a quarter-wave retarder and was sent under normal incidence onto the sample with a spot size of about 100 μm. The transmitted light was dispersed by another double monochromator and detected by a liquid-nitrogen cooled charge coupled device camera, providing a spectral resolution of about 10 μeV. Since the spectral width of the studied exciton resonances is significantly larger than this resolution, the setup provides sufficient resolution, as confirmed also by reference measurements with a tunable frequency-stabilized laser with neV resolution. The measurements with the two different light sources yielded identical spectra. The excitation density was chosen low enough that the excitation of dressed states, as discussed by Grünwald et al. [4], can be neglected and the observed spectral lines in the experiment correspond to resonant absorption peaks.

For an overview, we give in Fig. 1 a contour plot of absorption spectra composed by superposition of counter-circularly polarized spectra to show all optically accessible
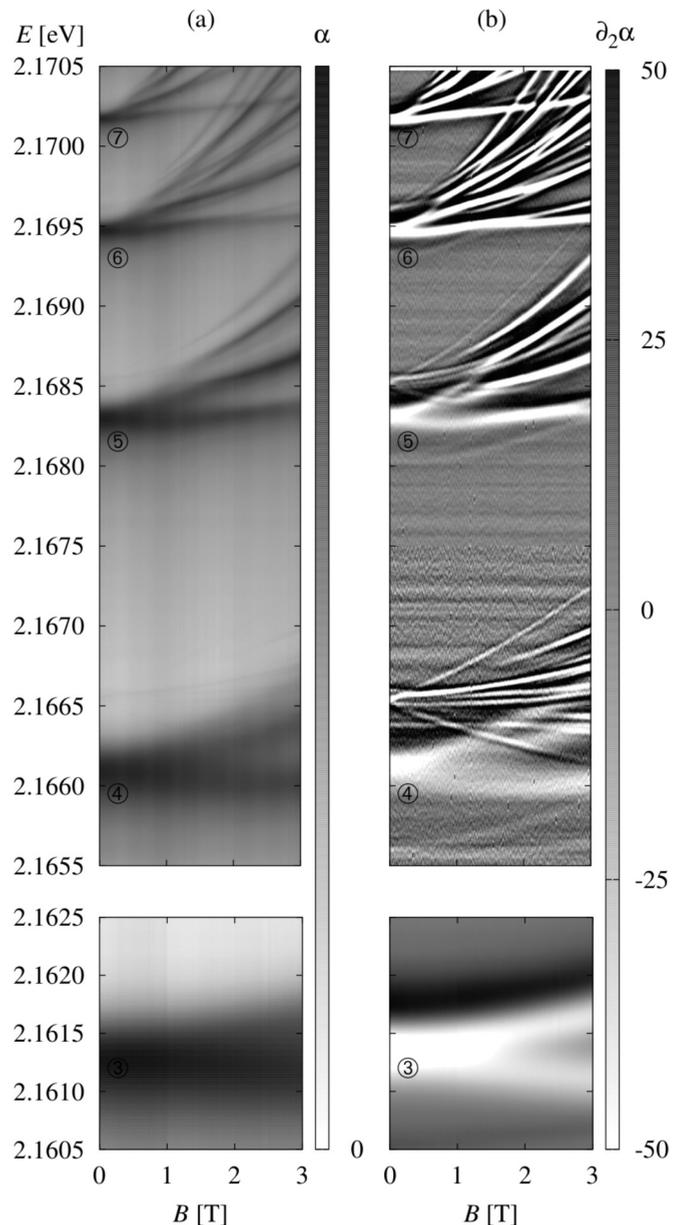

FIG. 1. (a) Absorption spectra of the $n = 3 \ldots 7$ excitons in an external magnetic field $\boldsymbol{B} \parallel [001]$ composed by superposition of countercircularly polarized spectra. The absorption constant α is given in arbitrary units. (b) Second derivative of the experimental absorption. The value of $\partial_2 \alpha$ is given in arbitrary units. The second derivative levels intensity differences and thus highlights the contribution of exciton states with higher angular momentum L to the spectra. Note that the faint periodic horizontal patterns are artifacts arising from taking the second derivative of the spectra.

exciton states, recorded on the [001] oriented sample. The energy range from the $n = 3$ exciton around 2.162 eV up to $n = 7$ on the high energy side is displayed. The left hand plot shows the absorption as recorded, and the right hand side shows the second derivative of the recorded spectra which helps to level intensity differences between features and highlight weak absorption lines. At zero field the spectra are dominated by the dipole-allowed P excitons [6,8]. With increasing magnetic field, each P exciton shows mostly a

doublet splitting. Simultaneously on their high energy flanks new lines emerge and become steadily stronger. Except of the magnitude of the splitting, the appearance of the $n = 4$ multiplet is somewhat similar to that of the $n = 5$ multiplet, involving also a similar number of lines. By contrast, the $n = 6$ multiplet is composed of many more lines due to the presence of exciton states with angular momentum $L = 5$.

In general, the impact of the magnetic field in terms of shifting and splitting levels grows with increasing principal quantum number n due to the increased extension of the exciton wave function,

$$r_{n,L} = \tfrac{1}{2} a_{\mathrm{exc}} (3n^2 - L(L+1)), \tag{34}$$

with the exciton Bohr radius $a_{\mathrm{exc}} = 1.11$ nm and envelope angular momentum L, compared to the magnetic length

$$\ell_c = \sqrt{\frac{\hbar}{eB}} = \frac{25.6 \text{ nm}}{\sqrt{B\,[\mathrm{T}]}}. \tag{35}$$

For example, the diamagnetic shift of the center-of-gravity of a line multiplet belonging to a specific n, which is a measure of the wave function extension normal to the field, increases from less than 0.1 meV for $n = 3$ up to $B = 3$ T (see below) to about 0.5 meV for $n = 5$. Furthermore, due to the reduced energy splitting between exciton multiplets and their extended Zeeman splitting in a magnetic field for higher n, exciton states belonging to different principal quantum numbers come into resonance at smaller magnetic field strengths. For example, the first resonance of two states belonging to $n = 5$ and $n = 6$ occurs at about 3.5 T, while the corresponding resonance between the $n = 6$ and the $n = 7$ multiplet occurs at 2 T.

We have shown recently that for $n > 6$ the electron-hole motion becomes chaotic in a magnetic field, as confirmed by corresponding theoretical calculations [2,12]. In the chaos regime the density of states is so high that an exact identification of the individual exciton states, while still being distinguishable, becomes increasingly complex as does the theoretical calculation. Instead statistical methods can be applied, such as the calculation of the level spacing distribution which transfers from a Poissonian to a Wigner-Dyson distribution going from the regular to the chaotic motion regime. The Wigner-Dyson distribution function is characterized by the dominance of avoided crossings between levels while crossings are suppressed. For $n \leqslant 6$ we observe in our measurements a clear dominance of crossings, confirming that in this range the motion stays regular. In combination with the possibility to assign the exciton character, we therefore restrict to $n \leqslant 5$ here.

To obtain more detailed insight into the level splitting in a magnetic field, we focus on exciton multiplets belonging to a particular n. Moreover, we consider circularly polarized spectra with the goal to reduce the number of exciton lines in a spectrum. Figure 2 shows contour plots of absorption spectra for $\boldsymbol{B} \parallel [001]$ in the energy range of the $n = 3$ and $n = 5$ excitons, in one panel for left circular polarization of the white light, and in the other panel for right circular polarization. Again, also the second derivatives of the absorption spectra are shown (see Fig. 3). The $n = 3$ exciton, for which the envelope angular momentum L is limited to 2, is characterized by the doublet splitting of the P exciton. The faint features from
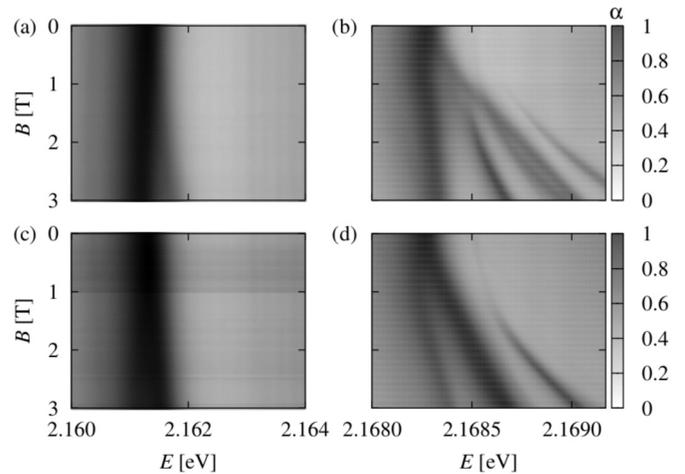
the S and D excitons due to quadrupole-allowed transitions also show a doublet splitting. We note that the relative oscillator strengths to a good approximation do not change with magnetic field, which indicates that as expected these excitons do not become mixed with the P excitons. For completeness we stress again that in a crystal orbital angular momentum strictly speaking is no good quantum number, but the discrete symmetry leads to a mixing of states with different L, in particular of the S and the D excitons as well as the P and the F excitons. Still, for reasons of simplicity, we use these notations here.

FIG. 2. Absorption spectra of (left) $n = 3$ and (right) $n = 5$ excitons. The values of the absorption constant α are given in arbitrary units. The spectra were obtained in Faraday configuration with an external magnetic field $\boldsymbol{B} \parallel [001]$ and (above) σ^+ or (below) σ^- polarized light.
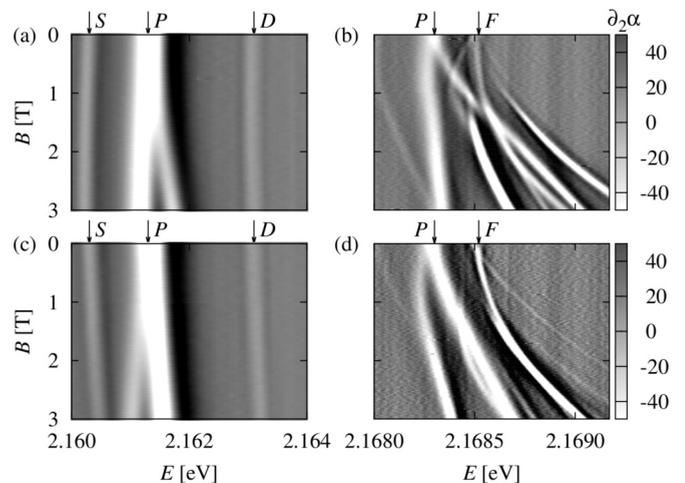

FIG. 3. Second derivative ($\partial_2 \alpha$) of the absorption spectra of Fig. 2. The values of $\partial_2 \alpha$ are given in arbitrary units. The large number of exciton lines for $n = 5$ and especially the zero-field splitting of P and F excitons can be seen more clearly in this presentation of the experimental results. We note that for the $n = 3$ exciton two more lines are observed in this presentation, which we attribute to the S exciton for the low energy line and the D exciton for the high energy line. We attribute their appearance to quadrupole-allowed transitions to the S exciton. For the D exciton quadrupole excitation is possible because of mixing with the S exciton [24].
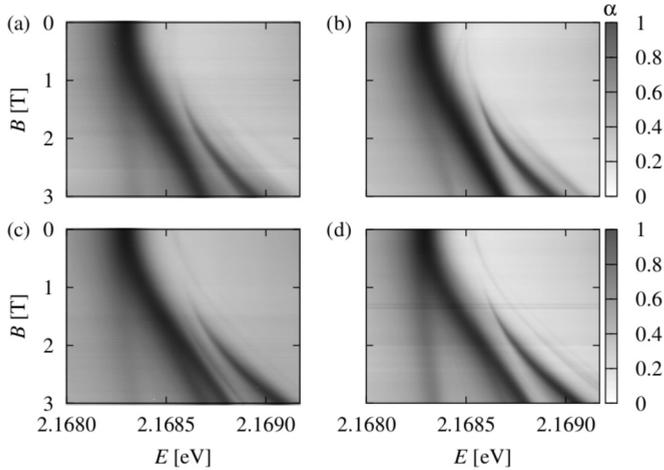
FIG. 4. Absorption spectra of the $n = 5$ exciton for (left) $\boldsymbol{B} \parallel$ [110] and (right) $\boldsymbol{B} \parallel$ [111]. The values of α are given in arbitrary units. Also for these orientations of the magnetic field, one can see a clear difference between the spectra for (above) σ^+ and (below) σ^- polarized light.
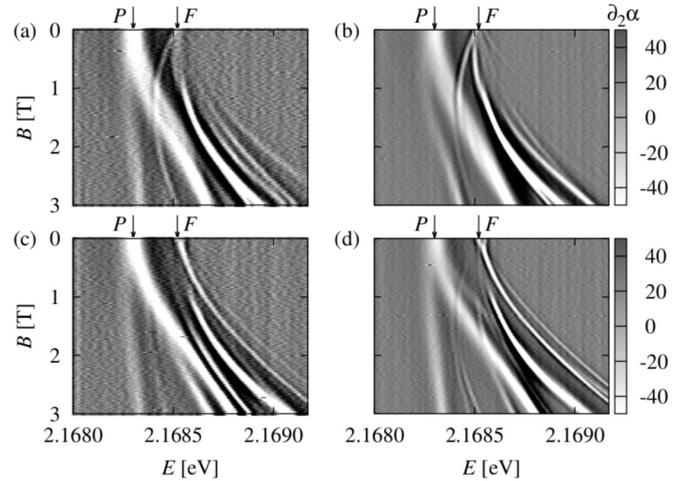

FIG. 5. Second derivative of the absorption spectra of Fig. 4. The values of $\partial_2 \alpha$ are given in arbitrary units. Again, the large number of exciton lines for $n = 5$ can be seen more clearly in this presentation of the experimental results.

The magnetic field induces and enhances the mixing of states with the same parity. This is clearly seen for the $n = 5$ exciton multiplet. At $B = 0$ T, besides the dominant P exciton the F excitons splitting to higher energies can be resolved, most prominently in the second derivative spectra due to their rather small relative oscillator strength (more than two orders of magnitude smaller than that of the P states). With increasing field the F excitons become much more prominent and also new lines from this multiplet emerge due to state mixing with the P excitons, from which oscillator strength is transferred. This allows us to obtain a detailed picture of the Zeeman-effect induced splitting of the different lines. Comparing the spectra for the two countercircular polarizations we note that they show distinct differences. This clearly shows that the often used description of an exciton by a hydrogen atom model is not appropriate, but the details of the electronic band structure need to be accounted for.

This is corroborated by the measurements in Figs. 4 and 5, showing corresponding measurements and second derivatives for the $n = 5$ exciton in the crystals with [110] and [111] orientation. Also here we find striking differences between the two countercircular polarizations. Moreover, they are also different compared to the spectra for the [001] field orientation. Also indications for anticrossings together with the corresponding exchange of oscillator strength can be observed in the field dispersion; see, for example, the σ^--polarized spectrum in the lower right panel of Fig. 5.

We note that for the [001] orientation a perfect circular polarization of the transitions is expected, so that excitation with particular helicity in principle can be used for optical orientation of the electron spin. However, when calculating the degree of circular polarization defined as

$$\rho_c(E) = \frac{\alpha_{\sigma^-} - \alpha_{\sigma^+}}{\alpha_{\sigma^-} + \alpha_{\sigma^+}}, \qquad (36)$$

where α_{σ^-} and α_{σ^+} are the absorption as function of energy for σ^- and σ^+ polarization, respectively, we find polarization

degrees well below unity but they are limited to values between $-0.3 < \rho_c < 0.5$, as seen from Fig. 6. This reduced polarization is the result of the finite width of the lines leading to spectral overlap. Note that for the other field orientation such as along [110] the polarization of the optical transitions is expected to be more complex.

V. RESULTS AND DISCUSSION

First we determine the maximum number of dipole-allowed exciton states via group theoretical considerations. In this way, we can also show that the external magnetic field lifts all degeneracies of the exciton states. In the spherical approximation, in which the cubic part of the Hamiltonian is neglected, the angular momentum F is a good quantum number. However, if the complete Hamiltonian is treated, the reduction of the irreducible representations D^F of the rotation group by the cubic group O_h has to be considered [40]. As has already been stated in Sec. III, a normal spin one transforms according to the irreducible representation Γ_4^+ of the cubic group and the quasispin I transforms according to $\Gamma_5^+ = \Gamma_4^+ \otimes \Gamma_2^+$. Therefore, one has to include the additional factor Γ_2^+ when determining the symmetry of an exciton state [6,8,24]. This symmetry is given by the symmetry of the
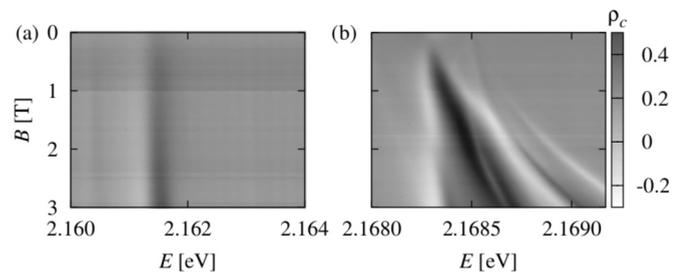

FIG. 6. Degree of circular polarization ρ_c of (a) $n = 3$ and (b) $n = 5$ excitons for $\boldsymbol{B} \parallel$ [001]. It can be seen that none of the observed lines shows complete circular polarization.
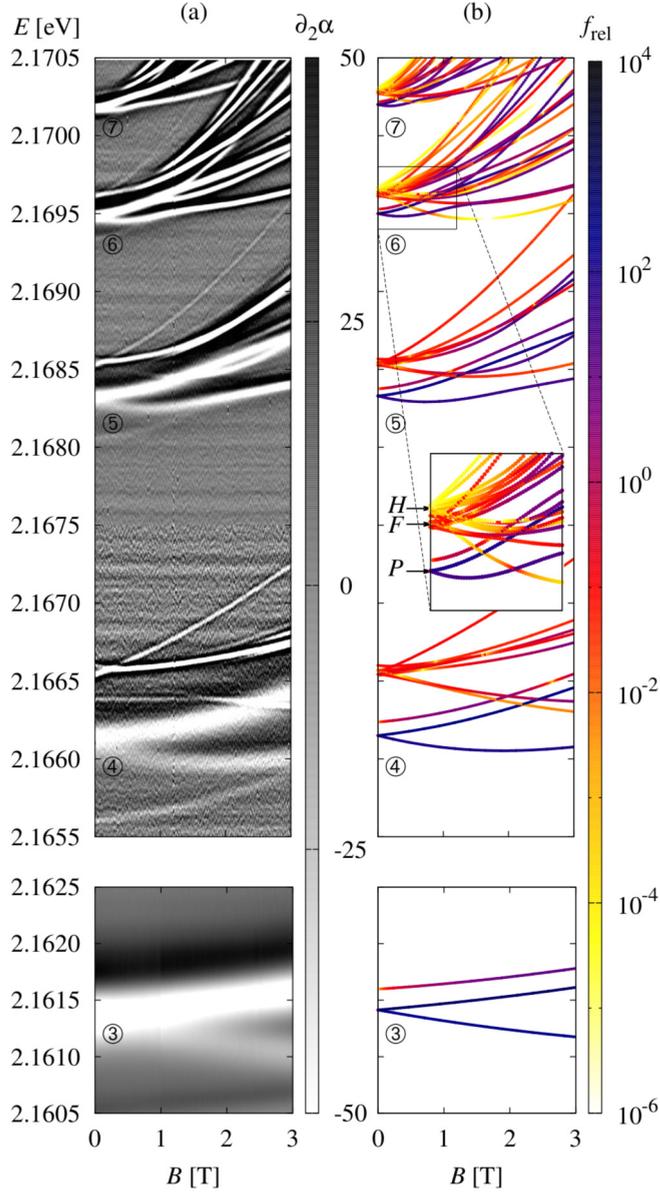
FIG. 7. Spectra of the $n = 3 \dots 7$ excitons in an external magnetic field $\boldsymbol{B} \parallel [001]$ for σ^- polarized light. (a) Second derivative of the experimental absorption spectrum. The value of $\partial_2 \alpha$ is given in arbitrary units. (b) Theoretical line spectrum for $\kappa = -0.5$. The color bar shows the calculated relative oscillator strength in arbitrary units. Since the complete Hamiltonian mixes exciton states with odd angular momentum, we expect the appearance of F excitons for $n \geqslant 4$ and H excitons for $n \geqslant 6$ as can be clearly seen, e.g., in the inset in panel (b).

envelope function, the valence band, and the conduction band:

$$\Gamma_{\mathrm{exc}} = \Gamma_{\mathrm{env}} \otimes \Gamma_{\mathrm{v}} \otimes \Gamma_{\mathrm{c}}. \tag{37}$$

As the quasispin I already enters the angular momentum F, we obtain the combined symmetry of the envelope function and the hole in the reduction of the representations D^F of the full rotation group:

$$\tilde{D}^{\frac{1}{2}} = D^{\frac{1}{2}} \otimes \Gamma_2^+ = \Gamma_6^- \otimes \Gamma_2^+ = \Gamma_7^-, \tag{38a}$$

$$\tilde{D}^{\frac{3}{2}} = D^{\frac{3}{2}} \otimes \Gamma_2^+ = \Gamma_8^- \otimes \Gamma_2^+ = \Gamma_8^-, \tag{38b}$$
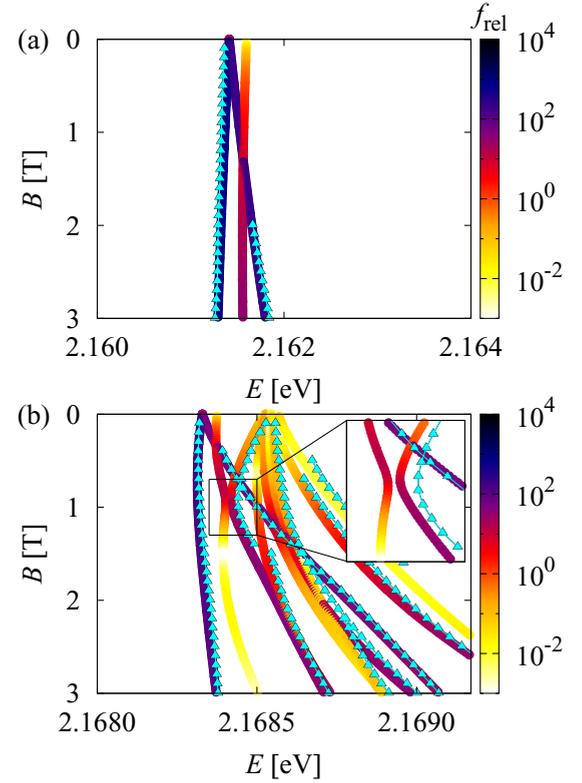

FIG. 8. Theoretical line spectrum of the (a) $n = 3$ and (b) $n = 5$ exciton states in an external magnetic field $\boldsymbol{B} \parallel [001]$ for σ^+ polarized light. The color bar shows the calculated relative oscillator strength in arbitrary units. The inset enlarges the most prominent anticrossing in the spectrum. This anticrossing involves the two exciton states, which originate from the Γ_7^- state of Eq. (38a) and the Γ_7^- state of Eq. (38d) at $B = 0\,\mathrm{T}$ (see also Ref. [8]). By comparing the theoretical results with the position of those exciton states, which could unambiguously be read out from the experimental spectrum (blue triangles) using the method of the second derivative [7], we can determine the fourth Luttinger parameter κ. An excellent agreement between theory and experiment is obtained for $\kappa = -0.50 \pm 0.10$. As the second derivative does not yield the exact position of the resonances, we have shifted the experimental spectrum by an amount of (a) 100 μeV and (b) 55 μeV.

$$\tilde{D}^{\frac{5}{2}} = D^{\frac{5}{2}} \otimes \Gamma_2^+ = (\Gamma_7^- \oplus \Gamma_8^-) \otimes \Gamma_2^+ = \Gamma_6^- \oplus \Gamma_8^-, \tag{38c}$$

$$\tilde{D}^{\frac{7}{2}} = D^{\frac{7}{2}} \otimes \Gamma_2^+ = (\Gamma_6^- \oplus \Gamma_7^- \oplus \Gamma_8^-) \otimes \Gamma_2^+$$
$$= \Gamma_7^- \oplus \Gamma_6^- \oplus \Gamma_8^-. \tag{38d}$$

It can be seen that there are two exciton states for $n = 2$ or $n = 3$ and seven exciton states for $n = 4$ or $n = 5$. Including the symmetry Γ_6^+ of the electron or the conduction band, the total symmetry of the exciton is

$$\Gamma_{\mathrm{exc}}^{\frac{1}{2}} = \tilde{D}^{\frac{1}{2}} \otimes \Gamma_6^+ = (\Gamma_2^- \oplus \Gamma_5^-), \tag{39a}$$

$$\Gamma_{\mathrm{exc}}^{\frac{3}{2}} = \tilde{D}^{\frac{3}{2}} \otimes \Gamma_6^+ = (\Gamma_3^- \oplus \Gamma_4^- \oplus \Gamma_5^-), \tag{39b}$$

$$\Gamma_{\mathrm{exc}}^{\frac{5}{2}} = \tilde{D}^{\frac{5}{2}} \otimes \Gamma_6^+ = (\Gamma_1^- \oplus \Gamma_4^-) \oplus (\Gamma_3^- \oplus \Gamma_4^- \oplus \Gamma_5^-), \tag{39c}$$
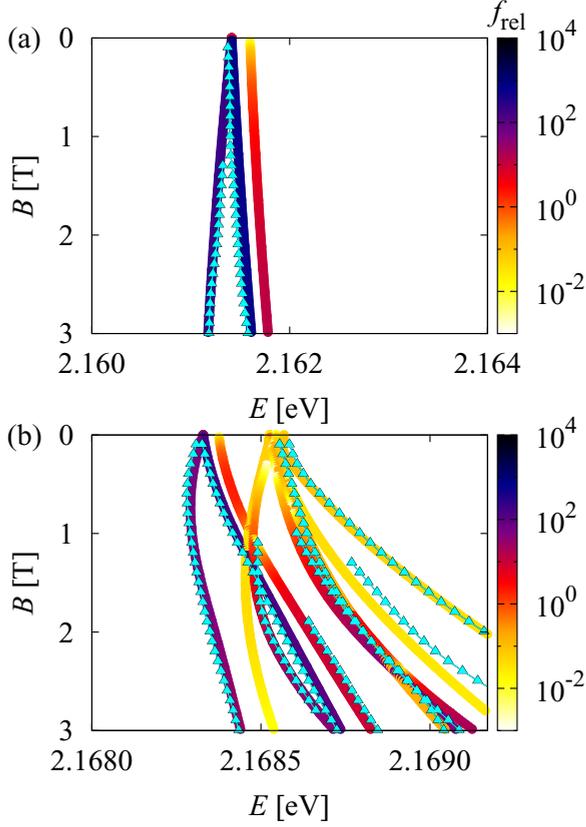
FIG. 9. Same comparison as in Fig. 8 but for σ^- polarized light. Again, we obtain an excellent agreement between theory and experiment for $\kappa = -0.50 \pm 0.10$.

$$
\begin{aligned}
\Gamma^{\frac{7}{2}}_{\text{exc}} &= \tilde{D}^{\frac{7}{2}} \otimes \Gamma^+_6 \\
&= (\Gamma^-_1 \oplus \Gamma^-_4) \oplus (\Gamma^-_2 \oplus \Gamma^-_5) \oplus (\Gamma^-_3 \oplus \Gamma^-_4 \oplus \Gamma^-_5),
\end{aligned}
$$

(39d)

respectively. Since the symmetries in parentheses belong to degenerate states, there are fourfold and eightfold degenerate states.

In the presence of a magnetic field being oriented along one of the crystal axes, we have to consider the reduction of the irreducible representations of the cubic group O_h by the group C_{4h} [41]:

$$
\Gamma^-_1 \to \Gamma^-_1, \tag{40a}
$$

$$
\Gamma^-_2 \to \Gamma^-_2, \tag{40b}
$$

$$
\Gamma^-_3 \to \Gamma^-_1 \oplus \Gamma^-_2, \tag{40c}
$$

$$
\Gamma^-_4 \to \Gamma^-_1 \oplus \Gamma^-_3 \oplus \Gamma^-_4, \tag{40d}
$$

$$
\Gamma^-_5 \to \Gamma^-_2 \oplus \Gamma^-_3 \oplus \Gamma^-_4. \tag{40e}
$$

Inserting these relations in Eq. (39), we see that degeneracies are further lifted. Since all irreducible representations of C_{4h} are one dimensional, we expect that all degeneracies are lifted so that there are 12 exciton states for $n = 2$ or $n = 3$ and 40 exciton states for $n = 4$ or $n = 5$. Since only the states with the symmetry Γ^-_3 and Γ^-_4 are dipole allowed, we immediately see that out of these only six states are dipole allowed for $n = 2$ or $n = 3$ and 20 for $n = 4$ or $n = 5$.
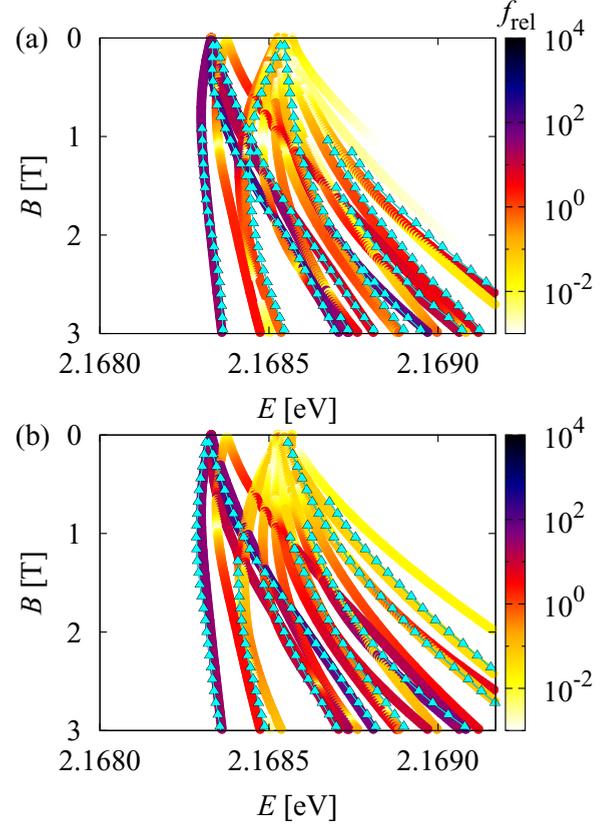
FIG. 10. Theoretical line spectrum of the $n = 5$ exciton states in an external magnetic field $\boldsymbol{B} \parallel [110]$ for (a) σ^+ and (b) σ^- polarized light. The color bar shows the calculated relative oscillator strength in arbitrary units. The exciton states, which could unambiguously be read out from the experiment are again marked by blue triangles. Since σ^+ and σ^- polarized light belong to the same irreducible representation of C_{2h}, it is possible to excite a certain exciton state by σ^+ *and* by σ^- polarized light. Hence all 20 dipole-allowed exciton states can be observed in panel (a) and in panel (b). Note that we have shifted the experimental spectrum by an amount of 26 μeV.

In the same manner we can also treat the special cases of a magnetic field being oriented along the [110] and the [111] direction, i.e., we have to consider the reduction of the irreducible representations of the cubic group O_h by the groups C_{2h} and C_{3i} [41]. Since all irreducible representations of these groups are one dimensional we also expect that all degeneracies are lifted and that there are 12 exciton states for $n = 2$ or $n = 3$ and 40 exciton states for $n = 4$ or $n = 5$. However, if we consider only the number of dipole-allowed states we find that there are 6 ($n = 2, 3$) and 20 ($n = 4, 5$) dipole-allowed states for $\boldsymbol{B} \parallel [110]$, but 8 ($n = 2, 3$) and 26 ($n = 4, 5$) dipole-allowed states for $\boldsymbol{B} \parallel [111]$.

For a first overview we show the experimental spectra for $\boldsymbol{B} \parallel [001]$ along with theoretical results for $n = 3 \dots 7$ in Fig. 7. In the special case of $\gamma_2 = \gamma_3 = \eta_i = 0$ the angular momentum L would be a good quantum number and due to the selection rules discussed in Sec. III only P excitons would be observable in this case. However, even without a magnetic field the complete Hamiltonian couples different exciton states with odd values of L so that also exciton states with higher
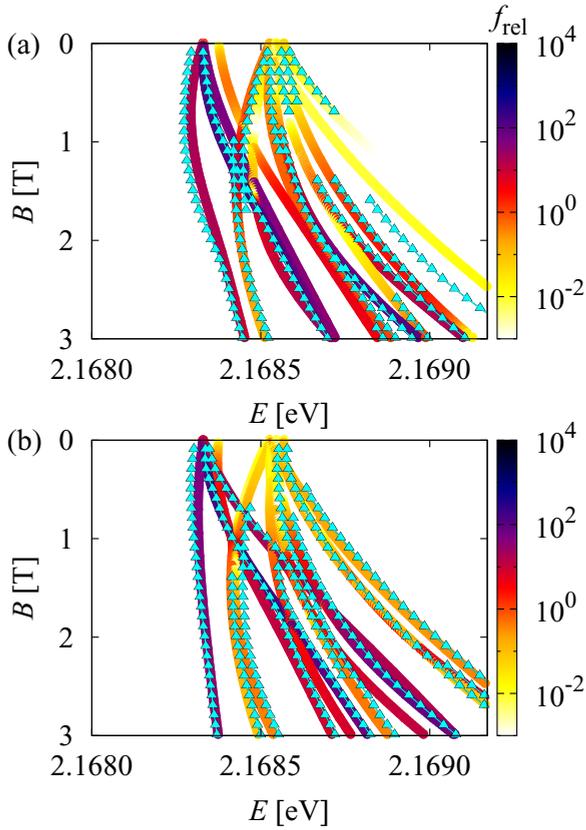
FIG. 11. Theoretical line spectrum of the $n = 5$ exciton states in an external magnetic field $\boldsymbol{B} \parallel [111]$ for (a) σ^+ and (b) σ^- polarized light. Note that we have shifted the experimental spectrum by an amount of 26 μeV.

angular momentum gain a small oscillator strength. This can be seen clearly from the theoretically calculated spectrum in panel (b) of Fig. 7.

Since $L \leqslant n - 1$ holds, the number of exciton lines for $n \geqslant 6$ is very high and a quantitative analysis is hardly possible. Hence we concentrate on the $n = 3$ and $n = 5$ exciton states in the following. The theoretical exciton spectra of these excitons in a magnetic field of $B \leqslant 3$ T with $\boldsymbol{B} \parallel [001]$ are depicted in Figs. 8 and 9 along with the exciton states read from experimental data. From Figs. 8(b) and 9(b) one can clearly distinguish between the contribution of the P excitons and the F excitons at $B = 0$ T [8]. It can be seen that the relative oscillator strength of F excitons significantly increases due to state mixing with growing field strength.

By comparing the experimentally observed line splitting to our results, we can estimate the value of the fourth Luttinger parameter to

$$\kappa = -0.50 \pm 0.10 \qquad (41)$$

provided that the values listed in Table I are correct (see also the according discussion in Ref. [8]). Using this value in our numerical calculations, we obtain an excellent agreement between theory and experiment for both $n = 3$ and $n = 5$ excitons in Figs. 8 and 9. The value of κ is further confirmed by the fact that only one exciton state can be observed at $B = 3$ T and $E \approx 2.1687$ eV in the experiment for σ^+ polarized light
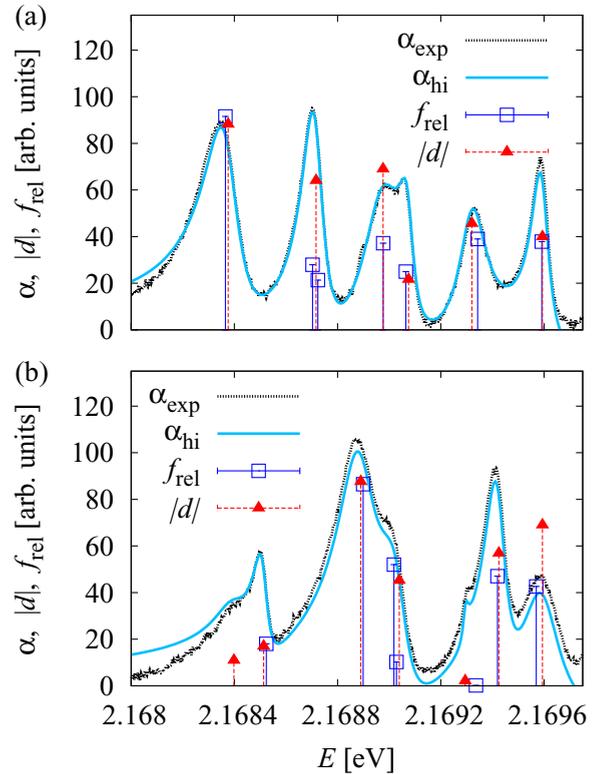

FIG. 12. Experimental spectrum (black dotted line) for $\boldsymbol{B} \parallel [001]$ analyzed using the method of harmonic inversion [45,46]. The panels show the spectra for (a) σ^+ polarized light at $B = 3$ T and (b) σ^- polarized light at $B = 4$ T. Since several exciton states are almost degenerate for σ^- polarized light at $B = 3$ T (cf. Fig. 9), we analyze the spectrum at $B = 4$ T. The positions and the amplitudes of the resonances obtained are marked by red triangles. The blue solid line shows the function $G(E)$ of Eq. (42) for these resonances. Note that in panel (a) the rightmost resonance originates from an $n = 6$ exciton state. Comparing the positions of the resonances to the theoretical spectrum (dark blue squares) yields the optimum values $\gamma_1 = 1.73 \pm 0.02$ and $\kappa = -0.50 \pm 0.10$ for the first and the fourth Luttinger parameter. Furthermore, we obtain a good agreement between the relative oscillator strengths f_{rel} and the modulus $|d|$ of amplitudes of the resonances.

(see Fig. 8). Only if $-0.52 < \kappa < -0.46$ holds, theory predicts two nearly degenerate states. For other values of κ, i.e., for $\kappa > -0.4$ or $\kappa < -0.6$, this degeneracy is lifted and two states should be observable in the experiment.

We can now use the value of $\kappa = -0.50$ to calculate the exciton spectra for $\boldsymbol{B} \parallel [110]$ and $\boldsymbol{B} \parallel [111]$. The results are shown in Figs. 10 and 11. We observe not only an excellent agreement with the experimental results but also see a clear difference between the spectra for the different orientations of the magnetic field. This difference is caused only by the cubic part of the exciton Hamiltonian [see Eqs. (2) and (7)]. We also note that the number of exciton states, which can be observed with σ^+ and σ^- polarized light, differs. Especially for $\boldsymbol{B} \parallel [110]$ σ^+ and σ^- polarized light belong to the same irreducible representation of C_{2h}. Hence it is possible to excite a certain exciton state by σ^+ *and* by σ^- polarized light, for which reason all 20 dipole-allowed exciton states can be observed in Fig. 10(a) and in Fig. 10(b).

To compare the theoretically calculated relative oscillator strengths with the experimental values, we analyze the experimental spectra using the method of harmonic inversion, which is presented in detail in Refs. [45,46]. Within the harmonic inversion the spectra are Fourier transformed to find the positions $\text{Re}(E_k)$, widths $\text{Im}(E_k)$, and complex amplitudes d_k of underlying resonances. The spectrum can then be expressed by a sum of Lorentzians

$$G(E) = \text{Im}\left(\sum_k \frac{d_k}{E - E_k} \right). \tag{42}$$

The results are presented in Fig. 12. For σ^+ and σ^- polarized light one can identify six resonances with exciton states in the theoretical spectrum. For almost all of these resonances we obtain a very good agreement between the modulus $|d|$ of their amplitudes and the theoretically calculated relative oscillator strengths.

The harmonic inversion supplies the true position of the resonances, which is generally not identical to the position of the transmission minima due to the asymmetry of the exciton absorption peaks [1,3]. Hence we can compare the results for $\text{Re}(E_k)$ directly to the positions of the exciton states in the theoretical spectrum. This allows us not only to confirm the value of $\kappa = -0.50 \pm 0.10$ but also to determine the first Luttinger parameter more accurately. The best agreements are obtained for $\gamma_1 = 1.73 \pm 0.02$.

VI. SUMMARY AND OUTLOOK

We presented the theory to calculate exciton spectra in Faraday configuration in a uniform external magnetic field. Only by taking into account the complex valence band structure of Cu$_2$O, we could obtain an excellent agreement between theory and experiment as regards not only the relative position but also the relative oscillator strengths of the exciton states. In particular, we showed the significant differences between the spectra for different orientations of the external magnetic field. Comparing the theoretical spectrum for $n = 3$ and $n = 5$ excitons with experimental results and using the method of harmonic inversion, we were able to determine the fourth Luttinger parameter of cuprous oxide to $\kappa = -0.50 \pm 0.10$. As a next step, we plan to investigate the spectra of excitons in Cu$_2$O in crossed electric and magnetic fields.

APPENDIX A: HAMILTONIAN

In this section we give the Hamiltonian (7) in terms of irreducible tensors for the case that the magnetic field is oriented along the [001], [110], or [111] direction [8,32,36,37]. Note that we rotate the coordinate system to make the quantization axis or z axis coincide with the direction of the magnetic field. Hence we rotate the coordinate system by the Euler angles $(\alpha, \beta, \gamma) = (\pi, \pi/2, \pi/4)$ for $\boldsymbol{B} \parallel [110]$ and by $(\alpha, \beta, \gamma) = (0, \arccos(1/\sqrt{3}), \pi/4)$ for $\boldsymbol{B} \parallel [111]$.

The first-order and second-order tensor operators used in the following correspond, as in Ref. [32], to the vector operators $\boldsymbol{r}$, $\boldsymbol{L} = \boldsymbol{r} \times \boldsymbol{p}$, $\boldsymbol{I}$, $\boldsymbol{S}_{\text{e/h}}$ and to the second-rank Cartesian operators

$$I_{mn} = 3\{I_m, I_n\} - \delta_{mn} I^2, \tag{A1a}$$

$$P_{mn} = 3\{p_m, p_n\} - \delta_{mn} p^2, \tag{A1b}$$

$$-i M_{mn} = 3\{r_m, p_n\} - \delta_{mn} \boldsymbol{r}\,\boldsymbol{p}, \tag{A1c}$$

$$X_{mn} = 3\{r_m, r_n\} - \delta_{mn} r^2, \tag{A1d}$$

respectively. We also use the abbreviation

$$D_k^{(2)} = \left[I^{(1)} \times S_{\text{h}}^{(1)} \right]_k^{(2)}. \tag{A2}$$

The coefficients γ_1', μ', and δ' are given by [24,37]

$$\gamma_1' = \gamma_1 + \frac{m_0}{m_{\text{e}}}, \quad \mu' = \frac{6\gamma_3 + 4\gamma_2}{5\gamma_1'}, \quad \delta' = \frac{\gamma_3 - \gamma_2}{\gamma_1'}, \tag{A3}$$

and we define by analogy [8]

$$\nu = \frac{6\eta_3 + 4\eta_2}{5\eta_1}, \quad \tau = \frac{\eta_3 - \eta_2}{\eta_1}. \tag{A4}$$

Furthermore, we write the Hamiltonian in the form

$$H = H_0 + (eB)H_1 + (eB)^2 H_2. \tag{A5}$$

The expressions for H_0, H_1, and H_2 are given in the following.

1. Magnetic field in [001] direction

$$
\begin{aligned}
H_0 = {} & E_{\text{g}} - \frac{e^2}{4\pi\varepsilon_0\varepsilon}\frac{1}{r} + \frac{2}{3}\Delta\left(1 + \frac{1}{\hbar^2}I^{(1)} \cdot S_{\text{h}}^{(1)}\right) \\
& + \frac{\gamma_1'}{2\hbar^2 m_0}\left\{\hbar^2 p^2 - \frac{\mu'}{3}(P^{(2)} \cdot I^{(2)}) + \frac{\delta'}{3}\left(\sum_{k=\pm 4}[P^{(2)} \times I^{(2)}]_k^{(4)} + \frac{\sqrt{70}}{5}[P^{(2)} \times I^{(2)}]_0^{(4)}\right)\right\} \\
& + \frac{3\eta_1}{\hbar^2 m_0}\left\{\frac{1}{3}p^2\left(I^{(1)} \cdot S_{\text{h}}^{(1)}\right) - \frac{\nu}{3}(P^{(2)} \cdot D^{(2)}) + \frac{\tau}{3}\left(\sum_{k=\pm 4}[P^{(2)} \times D^{(2)}]_k^{(4)} + \frac{\sqrt{70}}{5}[P^{(2)} \times D^{(2)}]_0^{(4)}\right)\right\},
\end{aligned}
\tag{A6a}
$$

$$H_1 = \frac{1}{m_{\mathrm{e}}}L_0^{(1)} + \frac{\mu_{\mathrm{B}}}{e\hbar}\left(g_c S_{\mathrm{e}0}^{(1)} - g_s S_{\mathrm{h}0}^{(1)} + \left(3\kappa + \frac{1}{2}g_s\right)I_0^{(1)}\right) + \frac{\gamma_1'}{2\hbar^2 m_0}\left\{-\hbar^2 L_0^{(1)} + \frac{\delta'}{3}\left([M^{(2)} \times I^{(2)}]_{-4}^{(4)} - [M^{(2)} \times I^{(2)}]_4^{(4)}\right)\right.$$

$$+ \sqrt{\frac{2}{5}}\delta'\left([L^{(1)} \times I^{(2)}]_0^{(3)} - \frac{1}{3}[M^{(2)} \times I^{(2)}]_0^{(3)}\right) + \sqrt{\frac{5}{12}}\mu'\left([L^{(1)} \times I^{(2)}]_0^{(1)} + \sqrt{\frac{2}{3}}[M^{(2)} \times I^{(2)}]_0^{(1)}\right)\right\}$$

$$+ \frac{3\eta_1}{\hbar^2 m_0}\left\{-\frac{1}{3}L_0^{(1)}\left(I^{(1)} \cdot S_{\mathrm{h}}^{(1)}\right) + \frac{\tau}{3}\left([M^{(2)} \times D^{(2)}]_{-4}^{(4)} - [M^{(2)} \times D^{(2)}]_4^{(4)}\right) + \sqrt{\frac{2}{5}}\tau\left([L^{(1)} \times D^{(2)}]_0^{(3)} - \frac{1}{3}[M^{(2)} \times D^{(2)}]_0^{(3)}\right)\right.$$

$$+ \sqrt{\frac{5}{12}}\nu\left([L^{(1)} \times D^{(2)}]_0^{(1)} + \sqrt{\frac{2}{3}}[M^{(2)} \times D^{(2)}]_0^{(1)}\right)\right\}, \tag{A6b}$$

$$H_2 = \frac{\gamma_1'}{24\hbar^2 m_0}\left\{\hbar^2\left(2r^2 - \sqrt{\frac{2}{3}}X_0^{(2)}\right) - \delta'\left(\sum_{k=\pm 4}[X^{(2)} \times I^{(2)}]_k^{(4)} - \frac{2}{\sqrt{70}}[X^{(2)} \times I^{(2)}]_0^{(4)}\right)\right.$$

$$+ \frac{\sqrt{14}}{3}\left(\mu' - \frac{12}{35}\delta'\right)[X^{(2)} \times I^{(2)}]_0^{(2)} + \frac{\mu'}{3}(X^{(2)} \cdot I^{(2)}) + \sqrt{\frac{2}{3}}\left(\mu' - \frac{6}{5}\delta'\right)r^2 I_0^{(2)}\right\}$$

$$+ \frac{\eta_1}{4\hbar^2 m_0}\left\{\frac{1}{3}\left(2r^2 - \sqrt{\frac{2}{3}}X_0^{(2)}\right)\left(I^{(1)} \cdot S_{\mathrm{h}}^{(1)}\right) - \tau\left(\sum_{k=\pm 4}[X^{(2)} \times D^{(2)}]_k^{(4)} - \frac{2}{\sqrt{70}}[X^{(2)} \times D^{(2)}]_0^{(4)}\right)\right.$$

$$+ \frac{\sqrt{14}}{3}\left(\nu - \frac{12}{35}\tau\right)[X^{(2)} \times D^{(2)}]_0^{(2)} + \frac{\nu}{3}(X^{(2)} \cdot D^{(2)}) + \sqrt{\frac{2}{3}}\left(\nu - \frac{6}{5}\tau\right)r^2 D_0^{(2)}\right\}. \tag{A6c}$$

2. Magnetic field in [110] direction

$$H_0 = E_{\mathrm{g}} - \frac{e^2}{4\pi\varepsilon_0\varepsilon}\frac{1}{r} + \frac{2}{3}\Delta\left(1 + \frac{1}{\hbar^2}I^{(1)} \cdot S_{\mathrm{h}}^{(1)}\right) + \frac{\gamma_1'}{2\hbar^2 m_0}\left\{\hbar^2 p^2 - \frac{\mu'}{3}(P^{(2)} \cdot I^{(2)}) + \frac{\delta'}{4}\left(\sum_{k=\pm 4}[P^{(2)} \times I^{(2)}]_k^{(4)}\right)\right.$$

$$\left.- \frac{\sqrt{7}}{6}\delta'\left(\sum_{k=\pm 2}[P^{(2)} \times I^{(2)}]_2^{(4)} + \sqrt{\frac{1}{10}}[P^{(2)} \times I^{(2)}]_0^{(4)}\right)\right\} + \frac{3\eta_1}{\hbar^2 m_0}\left\{\frac{1}{3}p^2\left(I^{(1)} \cdot S_{\mathrm{h}}^{(1)}\right) - \frac{\nu}{3}(P^{(2)} \cdot D^{(2)})\right.$$

$$+ \frac{\tau}{4}\left(\sum_{k=\pm 4}[P^{(2)} \times D^{(2)}]_k^{(4)}\right) - \frac{\sqrt{7}}{6}\tau\left(\sum_{k=\pm 2}[P^{(2)} \times D^{(2)}]_k^{(4)} + \sqrt{\frac{1}{10}}[P^{(2)} \times D^{(2)}]_0^{(4)}\right)\right\}, \tag{A7a}$$

$$H_1 = \frac{1}{m_{\mathrm{e}}}L_0^{(1)} + \frac{\mu_{\mathrm{B}}}{e\hbar}\left(g_c S_{\mathrm{e}0}^{(1)} - g_s S_{\mathrm{h}0}^{(1)} + \left(3\kappa + \frac{1}{2}g_s\right)I_0^{(1)}\right) + \frac{\gamma_1'}{2\hbar^2 m_0}\left\{-\hbar^2 L_0^{(1)} - \frac{\delta'}{16}\left(\sum_{k=\pm 4}k[M^{(2)} \times I^{(2)}]_k^{(4)}\right)\right.$$

$$+ \frac{\sqrt{7}}{24}\delta'\left(\sum_{k=\pm 2}k[M^{(2)} \times I^{(2)}]_k^{(4)}\right) + \frac{1}{4\sqrt{3}}\delta'\left(\sum_{k=\pm 2}[M^{(2)} \times I^{(2)}]_k^{(3)} + \sqrt{\frac{2}{15}}[M^{(2)} \times I^{(2)}]_0^{(3)}\right)$$

$$- \frac{\sqrt{3}}{4}\delta'\left(\sum_{k=\pm 2}[L^{(1)} \times I^{(2)}]_k^{(3)} + \sqrt{\frac{2}{15}}[L^{(1)} \times I^{(2)}]_0^{(3)}\right) + \frac{1}{2}\sqrt{\frac{5}{3}}\mu'\left([L^{(1)} \times I^{(2)}]_0^{(1)} + \sqrt{\frac{2}{3}}[M^{(2)} \times I^{(2)}]_0^{(1)}\right)\right\}$$

$$+ \frac{3\eta_1}{\hbar^2 m_0}\left\{-\frac{1}{3}L_0^{(1)}\left(I^{(1)} \cdot S_{\mathrm{h}}^{(1)}\right) - \frac{\tau}{16}\left(\sum_{k=\pm 4}k[M^{(2)} \times D^{(2)}]_k^{(4)}\right) + \frac{\sqrt{7}}{24}\tau\left(\sum_{k=\pm 2}k[M^{(2)} \times D^{(2)}]_k^{(4)}\right)\right.$$

$$+ \frac{1}{4\sqrt{3}}\tau\left(\sum_{k=\pm 2}[M^{(2)} \times D^{(2)}]_k^{(3)} + \sqrt{\frac{2}{15}}[M^{(2)} \times D^{(2)}]_0^{(3)}\right) - \frac{\sqrt{3}}{4}\tau\left(\sum_{k=\pm 2}[L^{(1)} \times D^{(2)}]_k^{(3)}\right.$$

$$\left.+ \sqrt{\frac{2}{15}}[L^{(1)} \times D^{(2)}]_0^{(3)}\right) + \frac{1}{2}\sqrt{\frac{5}{3}}\nu\left([L^{(1)} \times D^{(2)}]_0^{(1)} + \sqrt{\frac{2}{3}}[M^{(2)} \times D^{(2)}]_0^{(1)}\right)\right\}, \tag{A7b}$$

$$H_2 = \frac{\gamma_1'}{24\hbar^2 m_0}\left\{\hbar^2\left(2r^2 - \sqrt{\frac{2}{3}}X_0^{(2)}\right) - \frac{3}{4}\delta'\left(\sum_{k=\pm 4}[X^{(2)} \times I^{(2)}]_k^{(4)} + \frac{1}{3}\sqrt{\frac{2}{35}}[X^{(2)} \times I^{(2)}]_0^{(4)}\right)\right.$$

$$+ \frac{\delta'}{2\sqrt{7}}\left(\sum_{k=\pm 2}[X^{(2)} \times I^{(2)}]_k^{(4)}\right) + \frac{\delta'}{2\sqrt{3}}\left(\sum_{k=\pm 2}k[X^{(2)} \times I^{(2)}]_k^{(3)}\right) + \frac{\delta'}{\sqrt{21}}\left(\sum_{k=\pm 2}[X^{(2)} \times I^{(2)}]_k^{(2)}\right)$$

$$+ \frac{2}{3}\sqrt{\frac{7}{2}}\left(\mu' + \frac{3}{35}\delta'\right)[X^{(2)} \times I^{(2)}]_0^{(2)} + \frac{\mu'}{3}(X^{(2)} \cdot I^{(2)}) + \sqrt{\frac{2}{3}}\left(\mu' + \frac{3}{10}\delta'\right)r^2 I_0^{(2)} + \frac{\delta'}{2}r^2\left(I_2^{(2)} + I_{-2}^{(2)}\right)\right\}$$

$$+ \frac{\eta_1}{4\hbar^2 m_0}\left\{\frac{1}{3}\left(2r^2 - \sqrt{\frac{2}{3}}X_0^{(2)}\right)(I^{(1)} \cdot S_h^{(1)}) - \frac{3}{4}\tau\left(\sum_{k=\pm 4}[X^{(2)} \times D^{(2)}]_k^{(4)} + \frac{1}{3}\sqrt{\frac{2}{35}}[X^{(2)} \times D^{(2)}]_0^{(4)}\right)\right.$$

$$+ \frac{\tau}{2\sqrt{7}}\left(\sum_{k=\pm 2}[X^{(2)} \times D^{(2)}]_k^{(4)}\right) + \frac{\tau}{2\sqrt{3}}\left(\sum_{k=\pm 2}k[X^{(2)} \times D^{(2)}]_k^{(3)}\right) + \frac{\tau}{\sqrt{21}}\left(\sum_{k=\pm 2}[X^{(2)} \times D^{(2)}]_k^{(2)}\right)$$

$$+ \frac{2}{3}\sqrt{\frac{7}{2}}\left(\nu + \frac{3}{35}\tau\right)[X^{(2)} \times D^{(2)}]_0^{(2)} + \frac{1}{3}\nu(X^{(2)} \cdot D^{(2)}) + \sqrt{\frac{2}{3}}\left(\nu + \frac{3}{10}\tau\right)r^2 D_0^{(2)} + \frac{\tau}{2}r^2\left(D_2^{(2)} + D_{-2}^{(2)}\right)\right\}. \quad \text{(A7c)}$$

3. Magnetic field in [111] direction

$$H_0 = E_g - \frac{e^2}{4\pi\varepsilon_0\varepsilon}\frac{1}{r} + \frac{2}{3}\Delta\left(1 + \frac{1}{\hbar^2}I^{(1)} \cdot S_h^{(1)}\right)$$

$$+ \frac{\gamma_1'}{2\hbar^2 m_0}\left\{\hbar^2 p^2 - \frac{\mu'}{3}(P^{(2)} \cdot I^{(2)}) + \frac{4}{27}\delta'\left(\sum_{k=\pm 3}k[P^{(2)} \times I^{(2)}]_k^{(4)} - 3\sqrt{\frac{7}{10}}[P^{(2)} \times I^{(2)}]_0^{(4)}\right)\right\}$$

$$+ \frac{3\eta_1}{\hbar^2 m_0}\left\{\frac{1}{3}p^2\left(I^{(1)} \cdot S_h^{(1)}\right) - \frac{\nu}{3}(P^{(2)} \cdot D^{(2)}) + \frac{4}{27}\tau\left(\sum_{k=\pm 3}k[P^{(2)} \times D^{(2)}]_k^{(4)} - 3\sqrt{\frac{7}{10}}[P^{(2)} \times D^{(2)}]_0^{(4)}\right)\right\}, \quad \text{(A8a)}$$

$$H_1 = \frac{1}{m_e}L_0^{(1)} + \frac{\mu_B}{e\hbar}\left(g_c S_{e0}^{(1)} - g_s S_{h0}^{(1)} + \left(3\kappa + \frac{1}{2}g_s\right)I_0^{(1)}\right) + \frac{\gamma_1'}{2\hbar^2 m_0}\left\{-\hbar^2 L_0^{(1)} - \frac{\delta'}{3}\left(\sum_{k=\pm 3}[M^{(2)} \times I^{(2)}]_k^{(4)}\right)\right.$$

$$- \frac{\delta'}{27}\left(\sum_{k=\pm 3}k[M^{(2)} \times I^{(2)}]_k^{(3)} - 6\sqrt{\frac{2}{5}}[M^{(2)} \times I^{(2)}]_0^{(3)}\right) + \frac{\delta'}{9}\left(\sum_{k=\pm 3}k[L^{(1)} \times I^{(2)}]_k^{(3)} - 6\sqrt{\frac{2}{5}}[L^{(1)} \times I^{(2)}]_0^{(3)}\right)$$

$$+ \frac{1}{2}\sqrt{\frac{5}{3}}\mu'\left([L^{(1)} \times I^{(2)}]_0^{(1)} + \sqrt{\frac{2}{3}}[M^{(2)} \times I^{(2)}]_0^{(1)}\right)\right\} + \frac{3\eta_1}{\hbar^2 m_0}\left\{-\frac{1}{3}L_0^{(1)}\left(I^{(1)} \cdot S_h^{(1)}\right)\right.$$

$$- \frac{\tau}{3}\left(\sum_{k=\pm 3}[M^{(2)} \times D^{(2)}]_k^{(4)}\right) - \frac{\tau}{27}\left(\sum_{k=\pm 3}k[M^{(2)} \times D^{(2)}]_k^{(3)} - 6\sqrt{\frac{2}{5}}[M^{(2)} \times D^{(2)}]_0^{(3)}\right)$$

$$+ \frac{\tau}{9}\left(\sum_{k=\pm 3}k[L^{(1)} \times D^{(2)}]_k^{(3)} - 6\sqrt{\frac{2}{5}}[L^{(1)} \times D^{(2)}]_0^{(3)}\right) + \frac{1}{2}\sqrt{\frac{5}{3}}\nu\left([L^{(1)} \times D^{(2)}]_0^{(1)} + \sqrt{\frac{2}{3}}[M^{(2)} \times D^{(2)}]_0^{(1)}\right)\right\}, \quad \text{(A8b)}$$

$$H_2 = \frac{\gamma_1'}{24\hbar^2 m_0}\left\{\hbar^2\left(2r^2 - \sqrt{\frac{2}{3}}X_0^{(2)}\right) + \frac{2}{3}\delta'\left(-\frac{1}{3}\sum_{k=\pm 3}k[X^{(2)} \times I^{(2)}]_k^{(4)} - \sqrt{\frac{2}{35}}[X^{(2)} \times I^{(2)}]_0^{(4)}\right)\right.$$

$$- \frac{2}{3}\delta'\sum_{k=\pm 3}[X^{(2)} \times I^{(2)}]_k^{(3)} + \frac{2}{3}\sqrt{\frac{7}{2}}\left(\mu' + \frac{8}{35}\delta'\right)[X^{(2)} \times I^{(2)}]_0^{(2)} + \frac{\mu'}{3}(X^{(2)} \cdot I^{(2)}) + \sqrt{\frac{2}{3}}\left(\mu' + \frac{4}{5}\delta'\right)r^2 I_0^{(2)}\right\}$$

$$+ \frac{\eta_1}{4\hbar^2 m_0}\left\{\frac{1}{3}\left(2r^2 - \sqrt{\frac{2}{3}}X_0^{(2)}\right)(I^{(1)} \cdot S_h^{(1)}) + \frac{2}{3}\tau\left(-\frac{1}{3}\sum_{k=\pm 3}k[X^{(2)} \times I^{(2)}]_k^{(4)} - \sqrt{\frac{2}{35}}[X^{(2)} \times D^{(2)}]_0^{(4)}\right)\right.$$

$$- \frac{2}{3}\tau\sum_{k=\pm 3}[X^{(2)} \times I^{(2)}]_k^{(3)} + \frac{2}{3}\sqrt{\frac{7}{2}}\left(\nu + \frac{8}{35}\tau\right)[X^{(2)} \times D^{(2)}]_0^{(2)} + \frac{\nu}{3}(X^{(2)} \cdot D^{(2)}) + \sqrt{\frac{2}{3}}\left(\nu + \frac{4}{5}\tau\right)r^2 D_0^{(2)}\right\}. \quad \text{(A8c)}$$

APPENDIX B: OSCILLATOR STRENGTHS

We now give the formula for the expression

$$\lim_{r \to 0} \frac{\partial}{\partial r} \, {}_D\langle 2, M'_{F_t} | \Psi(\boldsymbol{r}) \rangle, \tag{B1}$$

which is needed for the evaluation of the relative oscillator strength f_{rel} (27). Using the wave function of Eq. (10), we find

$$
\lim_{r \to 0} \frac{\partial}{\partial r} \, {}_D\langle 2, M'_{F_t} | \Psi(\boldsymbol{r}) \rangle = \sum_{NJFF_t} \sum_{M_{S_e} M_I} c_{N1JFF_tM'_{F_t}} \frac{1}{3} \sqrt{\frac{10}{\alpha^5}} (-1)^{F-J-3M_{S_e}-M_I+3M'_{F_t}+\frac{3}{2}}
$$

$$
\times \, [(N+1)(N+3)(2J+1)(2F+1)(2F_t+1)]^{\frac{1}{2}} \begin{pmatrix} F & \frac{1}{2} & F_t \\ M'_{F_t}-M_{S_e} & M_{S_e} & -M'_{F_t} \end{pmatrix}
$$

$$
\times \begin{pmatrix} 1 & J & F \\ M'_{F_t}-M_I & M_I-M_{S_e} & M_{S_e}-M'_{F_t} \end{pmatrix} \begin{pmatrix} 1 & \frac{1}{2} & J \\ M_I & -M_{S_e} & M_{S_e}-M_I \end{pmatrix}
$$

$$
\times \begin{pmatrix} 1 & 1 & 2 \\ M_I & M'_{F_t}-M_I & -M'_{F_t} \end{pmatrix}. \tag{B2}
$$

APPENDIX C: MATRIX ELEMENTS

In this section we give the matrix elements of the terms of the Hamiltonian H [Eq. (A5)] in the basis of Eq. (10) in Hartree units using the formalism of irreducible tensors [36]. The matrix elements of the Hamiltonian H_0 [Eq. (A5)] are given in the Appendix of Ref. [8]. We use the abbreviation

$$\tilde{\delta}_{\Pi\Pi'} = \delta_{LL'}\delta_{JJ'}\delta_{FF'}\delta_{F_tF'_t}\delta_{M_{F_t}M'_{F_t}} \tag{C1}$$

in the following. The functions of the form $(R_1)_{nL}^j$ are taken from the recursion relations of the Coulomb-Sturmian functions in the Appendix of Ref. [8]:

$$\langle \Pi' | r^2 | \Pi \rangle = \tilde{\delta}_{\Pi\Pi'} \sum_{j=-3}^{3} (R_3)_{NL}^j [N+L+j+1]^{-1} \delta_{N',N+j}, \tag{C2}$$

$$
\langle \Pi' | r^2 I_q^{(2)} | \Pi \rangle = \delta_{LL'} 3\sqrt{5} (-1)^{F'_t+F_t-M'_{F_t}+2F'+L+2J} [(2F_t+1)(2F'_t+1)(2F+1)(2F'+1)(2J+1)(2J'+1)]^{\frac{1}{2}}
$$

$$
\times \begin{pmatrix} F'_t & 2 & F_t \\ -M'_{F_t} & q & M_{F_t} \end{pmatrix} \begin{Bmatrix} F' & F'_t & \frac{1}{2} \\ F_t & F & 2 \end{Bmatrix} \begin{Bmatrix} J' & F' & L \\ F & J & 2 \end{Bmatrix} \begin{Bmatrix} 1 & J' & \frac{1}{2} \\ J & 1 & \frac{1}{2} \end{Bmatrix} \sum_{j=-3}^{3} (R_3)_{NL}^j [N+L+j+1]^{-1} \delta_{N',N+j}, \tag{C3}
$$

$$
\langle \Pi' | X_q^{(2)} | \Pi \rangle = \delta_{JJ'} (-1)^{F'_t+F_t-M'_{F_t}+F'+F+L'+J+\frac{1}{2}} \langle N' \, L' \| X^{(2)} \| N \, L \rangle [(2F_t+1)(2F'_t+1)(2F+1)(2F'+1)]^{\frac{1}{2}}
$$

$$
\times \begin{pmatrix} F'_t & 2 & F_t \\ -M'_{F_t} & q & M_{F_t} \end{pmatrix} \begin{Bmatrix} F' & F'_t & \frac{1}{2} \\ F_t & F & 2 \end{Bmatrix} \begin{Bmatrix} L' & F' & J \\ F & L & 2 \end{Bmatrix}, \tag{C4}
$$

$$
\langle \Pi' | S_{e\,0}^{(1)} | \Pi \rangle = \delta_{LL'}\delta_{JJ'}\delta_{FF'}\delta_{M_{F_t}M'_{F_t}} \sqrt{\frac{3}{2}} (-1)^{2F'_t-M_{F_t}+F+\frac{3}{2}} [(2F_t+1)(2F'_t+1)]^{\frac{1}{2}} \begin{pmatrix} F'_t & 1 & F_t \\ -M_{F_t} & 0 & M_{F_t} \end{pmatrix}
$$

$$
\times \begin{Bmatrix} \frac{1}{2} & F'_t & F \\ F_t & \frac{1}{2} & 1 \end{Bmatrix} \sum_{j=-1}^{1} (R_1)_{NL}^j [N+L+j+1]^{-1} \delta_{N',N+j}, \tag{C5}
$$

$$
\langle \Pi' | S_{h\,0}^{(1)} | \Pi \rangle = \delta_{LL'}\delta_{M_{F_t}M'_{F_t}} \sqrt{\frac{3}{2}} (-1)^{F'_t+F_t-M_{F_t}+2F'+L+J+J'+1} [(2F_t+1)(2F'_t+1)(2F+1)(2F'+1)(2J+1)(2J'+1)]^{\frac{1}{2}}
$$

$$
\times \begin{pmatrix} F'_t & 1 & F_t \\ -M_{F_t} & 0 & M_{F_t} \end{pmatrix} \begin{Bmatrix} F' & F'_t & \frac{1}{2} \\ F_t & F & 1 \end{Bmatrix} \begin{Bmatrix} J' & F' & L \\ F & J & 1 \end{Bmatrix} \begin{Bmatrix} \frac{1}{2} & J' & 1 \\ J & \frac{1}{2} & 1 \end{Bmatrix} \sum_{j=-1}^{1} (R_1)_{NL}^j [N+L+j+1]^{-1} \delta_{N',N+j}, \tag{C6}
$$

$$
\langle \Pi' | L_0^{(1)} | \Pi \rangle = \delta_{LL'}\delta_{JJ'}\delta_{M_{F_t}M'_{F_t}} (-1)^{F'_t+F_t-M_{F_t}+F+F'+L+J+\frac{1}{2}} [(2F_t+1)(2F'_t+1)(2F+1)(2F'+1)L(L+1)(2L+1)]^{\frac{1}{2}}
$$

$$
\times \begin{pmatrix} F'_t & 1 & F_t \\ -M_{F_t} & 0 & M_{F_t} \end{pmatrix} \begin{Bmatrix} F' & F'_t & \frac{1}{2} \\ F_t & F & 1 \end{Bmatrix} \begin{Bmatrix} L & F' & J \\ F & L & 1 \end{Bmatrix} \sum_{j=-1}^{1} (R_1)_{NL}^j [N+L+j+1]^{-1} \delta_{N',N+j}, \tag{C7}
$$

$$\langle\Pi'|I_0^{(1)}|\Pi\rangle = \delta_{LL'}\delta_{M_{F_t}M'_{F_t}}\sqrt{6}(-1)^{F'_t+F_t-M_{F_t}+2F'+L+2J+1}[(2F_t+1)(2F'_t+1)(2F+1)(2F'+1)(2J+1)(2J'+1)]^{\frac{1}{2}}$$

$$\times \begin{pmatrix} F'_t & 1 & F_t \\ -M_{F_t} & 0 & M_{F_t} \end{pmatrix}\begin{Bmatrix} F' & F'_t & \frac{1}{2} \\ F_t & F & 1 \end{Bmatrix}\begin{Bmatrix} J' & F' & L \\ F & J & 1 \end{Bmatrix}\begin{Bmatrix} 1 & J' & \frac{1}{2} \\ J & 1 & 1 \end{Bmatrix}$$

$$\times \sum_{j=-1}^{1}(R_1)_{NL}^{j}[N+L+j+1]^{-1}\delta_{N',N+j}, \tag{C8}$$

$$\langle\Pi'|X^{(2)}\cdot I^{(2)}|\Pi\rangle = \sqrt{5}[X^{(2)}\times I^{(2)}]_0^{(0)}, \tag{C9}$$

$$\langle\Pi'|[M^{(2)}\times I^{(2)}]_q^{(K)}|\Pi\rangle = 3\sqrt{5}(-1)^{F'_t+F_t-M'_{F_t}+F'+J+K}\langle N'\,L'\|M^{(2)}\|N\,L\rangle$$

$$\times [(2F_t+1)(2F'_t+1)(2F+1)(2F'+1)(2K+1)(2J+1)(2J'+1)]^{\frac{1}{2}}$$

$$\times \begin{pmatrix} F'_t & K & F_t \\ -M'_{F_t} & q & M_{F_t} \end{pmatrix}\begin{Bmatrix} F' & F'_t & \frac{1}{2} \\ F_t & F & K \end{Bmatrix}\begin{Bmatrix} 1 & J' & \frac{1}{2} \\ J & 1 & 2 \end{Bmatrix}\begin{Bmatrix} L' & L & 2 \\ J' & J & 2 \\ F' & F & K \end{Bmatrix}, \tag{C10}$$

$$\langle\Pi'|[L^{(1)}I^{(2)}]_q^{(K)}|\Pi\rangle = \delta_{LL'}3\sqrt{5}(-1)^{F'_t+F_t-M'_{F_t}+F'+J+K}[L(L+1)(2L+1)]^{\frac{1}{2}}$$

$$\times [(2F_t+1)(2F'_t+1)(2F+1)(2F'+1)(2K+1)(2J+1)(2J'+1)]^{\frac{1}{2}}$$

$$\times \begin{pmatrix} F'_t & K & F_t \\ -M'_{F_t} & q & M_{F_t} \end{pmatrix}\begin{Bmatrix} F' & F'_t & \frac{1}{2} \\ F_t & F & K \end{Bmatrix}\begin{Bmatrix} 1 & J' & \frac{1}{2} \\ J & 1 & 2 \end{Bmatrix}\begin{Bmatrix} L' & L & 1 \\ J' & J & 2 \\ F' & F & K \end{Bmatrix}$$

$$\times \sum_{j=-1}^{1}(R_1)_{NL}^{j}[N+L+j+1]^{-1}\delta_{N',N+j}, \tag{C11}$$

$$\langle\Pi'|[X^{(2)}\times I^{(2)}]_q^{(K)}|\Pi\rangle = 3\sqrt{5}(-1)^{F'_t+F_t-M'_{F_t}+F'+J+K}\langle N'\,L'\|X^{(2)}\|N\,L\rangle[(2F_t+1)(2F'_t+1)(2F+1)(2F'+1)(2K+1)$$

$$\times (2J+1)(2J'+1)]^{\frac{1}{2}}\begin{pmatrix} F'_t & K & F_t \\ -M'_{F_t} & q & M_{F_t} \end{pmatrix}\begin{Bmatrix} F' & F'_t & \frac{1}{2} \\ F_t & F & K \end{Bmatrix}\begin{Bmatrix} 1 & J' & \frac{1}{2} \\ J & 1 & 2 \end{Bmatrix}\begin{Bmatrix} L' & L & 2 \\ J' & J & 2 \\ F' & F & K \end{Bmatrix},$$
$$\tag{C12}$$

$$\langle\Pi'|L_0^{(1)}(I^{(1)}\cdot S_{\mathrm{h}}^{(1)})|\Pi\rangle = \tfrac{1}{2}\big(J(J+1)-\tfrac{11}{4}\big)\langle\Pi'|L_0^{(1)}|\Pi\rangle, \tag{C13}$$

$$\langle\Pi'|r^2(I^{(1)}\cdot S_{\mathrm{h}}^{(1)})|\Pi\rangle = \tfrac{1}{2}\big(J(J+1)-\tfrac{11}{4}\big)\langle\Pi'|r^2|\Pi\rangle, \tag{C14}$$

$$\langle\Pi'|X_q^{(2)}(I^{(1)}\cdot S_{\mathrm{h}}^{(1)})|\Pi\rangle = \tfrac{1}{2}\big(J(J+1)-\tfrac{11}{4}\big)\langle\Pi'|X_q^{(2)}|\Pi\rangle, \tag{C15}$$

$$\langle\Pi'|r^2[I^{(1)}\times S_{\mathrm{h}}^{(1)}]_q^{(2)}|\Pi\rangle = \delta_{LL'}3\sqrt{5}(-1)^{F'_t+F_t-M'_{F_t}+2F'+L+J+\frac{1}{2}}[(2F_t+1)(2F'_t+1)(2F+1)(2F'+1)$$

$$\times (2J+1)(2J'+1)]^{\frac{1}{2}}\begin{pmatrix} F'_t & 2 & F_t \\ -M'_{F_t} & q & M_{F_t} \end{pmatrix}\begin{Bmatrix} F' & F'_t & \frac{1}{2} \\ F_t & F & 2 \end{Bmatrix}\begin{Bmatrix} J' & F' & L \\ F & J & 2 \end{Bmatrix}\begin{Bmatrix} 1 & 1 & 1 \\ \frac{1}{2} & \frac{1}{2} & 1 \\ J' & J & 2 \end{Bmatrix}$$

$$\times \sum_{j=-3}^{3}(R_3)_{NL}^{j}[N+L+j+1]^{-1}\delta_{N',N+j}, \tag{C16}$$

$$\langle\Pi'|X^{(2)}\cdot[I^{(1)}\times S_{\mathrm{h}}^{(1)}]^{(2)}|\Pi\rangle = \sqrt{5}\langle\Pi'|[X^{(2)}\times[I^{(1)}\times S_{\mathrm{h}}^{(1)}]^{(2)}]_0^{(0)}|\Pi\rangle, \tag{C17}$$

$$\langle\Pi'|[X^{(2)}\times[I^{(1)}\times S_{\mathrm{h}}^{(1)}]^{(2)}]_q^{(K)}|\Pi\rangle = 3\sqrt{5}(-1)^{F'_t+F_t-M'_{F_t}+F'+K+\frac{1}{2}}\langle N'\,L'\|X^{(2)}\|N\,L\rangle$$

$$\times [(2F_t+1)(2F'_t+1)(2F+1)(2F'+1)(2K+1)(2J+1)(2J'+1)]^{\frac{1}{2}}$$

$$\times \begin{pmatrix} F'_t & K & F_t \\ -M'_{F_t} & q & M_{F_t} \end{pmatrix}\begin{Bmatrix} F' & F'_t & \frac{1}{2} \\ F_t & F & K \end{Bmatrix}\begin{Bmatrix} L' & L & 2 \\ J' & J & 2 \\ F' & F & K \end{Bmatrix}\begin{Bmatrix} 1 & 1 & 1 \\ \frac{1}{2} & \frac{1}{2} & 1 \\ J' & J & 2 \end{Bmatrix}, \tag{C18}$$

$$
\langle \Pi'|\big[M^{(2)} \times \big[I^{(1)} \times S_{\mathrm{h}}^{(1)}\big]^{(2)}\big]_q^{(K)}|\Pi\rangle = 3\sqrt{5}(-1)^{F_t'+F_t-M_{F_t}'+F'+K+\frac{1}{2}} \langle N'\,L'\|M^{(2)}\|N\,L\rangle
$$

$$
\times \big[(2F_t+1)(2F_t'+1)(2F+1)(2F'+1)(2K+1)(2J+1)(2J'+1)\big]^{\frac{1}{2}}
$$

$$
\times \begin{pmatrix} F_t' & K & F_t \\ -M_{F_t}' & q & M_{F_t} \end{pmatrix} \begin{Bmatrix} F' & F_t' & \frac{1}{2} \\ F_t & F & K \end{Bmatrix} \begin{Bmatrix} L' & L & 2 \\ J' & J & 2 \\ F' & F & K \end{Bmatrix} \begin{Bmatrix} 1 & 1 & 1 \\ \frac{1}{2} & \frac{1}{2} & 1 \\ J' & J & 2 \end{Bmatrix}, \tag{C19}
$$

$$
\langle \Pi'|\big[L^{(1)} \times \big[I^{(1)} \times S_{\mathrm{h}}^{(1)}\big]^{(2)}\big]_q^{(K)}|\Pi\rangle = \delta_{LL'}3\sqrt{5}(-1)^{F_t'+F_t-M_{F_t}'+F'+K+\frac{1}{2}}\big[L(L+1)(2L+1)\big]^{\frac{1}{2}}
$$

$$
\times \big[(2F_t+1)(2F_t'+1)(2F+1)(2F'+1)(2K+1)(2J+1)(2J'+1)\big]^{\frac{1}{2}}
$$

$$
\times \begin{pmatrix} F_t' & K & F_t \\ -M_{F_t}' & q & M_{F_t} \end{pmatrix} \begin{Bmatrix} F' & F_t' & \frac{1}{2} \\ F_t & F & K \end{Bmatrix} \begin{Bmatrix} L' & L & 2 \\ J' & J & 2 \\ F' & F & K \end{Bmatrix} \begin{Bmatrix} 1 & 1 & 1 \\ \frac{1}{2} & \frac{1}{2} & 1 \\ J' & J & 2 \end{Bmatrix}
$$

$$
\times \sum_{j=-1}^{1} (R_1)_{NL}^{j}[N+L+j+1]^{-1}\delta_{N',N+j}. \tag{C20}
$$

APPENDIX D: REDUCED MATRIX ELEMENTS

We now list the values of the reduced matrix elements of the form $\langle N'\,L'\|A^{(j)}\|N\,L\rangle$. The functions of the form $(R_1)_{NL}^{j}$ and the integral $I_{N'L';NL}$ are taken from the Appendix of Ref. [8]:

$$
\langle N'\,L'\|X^{(2)}\|N\,L\rangle = \delta_{L',L+2}\frac{3}{2}\frac{1}{(L+1)(L+2)}\left[\prod_{j=1}^{5}(2L+j)\right]^{\frac{1}{2}}\left[\sum_{j=-5}^{1}\frac{(R_1LN_2)_{NL0}^{j\,2}}{(N+L+j+3)}\delta_{N',N+j}\right]
$$

$$
+ \delta_{L',L}\left(-\sqrt{\frac{3}{8}}\right)\frac{1}{L(L+1)}\left[\prod_{j=-1}^{3}(2L+j)\right]^{\frac{1}{2}}\left[\sum_{j=-3}^{3}\frac{3(R_1LN_2)_{NL0}^{j\,0}-(R_3)_{NL}^{j}}{(N+L+j+1)}\delta_{N',N+j}\right]
$$

$$
+ \delta_{L',L-2}\frac{3}{2}\frac{1}{L(L-1)}\left[\prod_{j=-3}^{1}(2L+j)\right]^{\frac{1}{2}}\left[\sum_{j=-1}^{5}\frac{(R_1LN_2)_{NL0}^{j-2}}{(N+L+j-1)}\delta_{N',N+j}\right], \tag{D1}
$$

$$
\langle N'\,L'\|M^{(2)}\|N\,L\rangle = \delta_{L',L+2}\frac{3}{2}\left[\frac{(2L+4)(2L+2)}{(2L+3)}\right]^{\frac{1}{2}}\left[\sum_{j=-3}^{3}(R_3P_1)_{NL}^{j}I_{N'L+2;N+jL} + \sum_{j=-2}^{2}\big(-L(R_2)_{NL}^{j}\big)I_{N'L+2;N+jL}\right]
$$

$$
+ \delta_{L',L}\left(-\frac{\sqrt{3}}{2}\right)\left[\frac{L(2L+1)(2L+2)}{(2L+3)(2L-1)}\right]^{\frac{1}{2}}
$$

$$
\times \left[\sum_{j=-2}^{2}\frac{2(R_2P_1)_{NL}^{j}}{(N+L+j+1)}\delta_{N',N+j} + \sum_{j=-1}^{1}\frac{3(R_1)_{NL}^{j}}{(N+L+j+1)}\delta_{N',N+j}\right] + \delta_{L',L-2}\frac{3}{2}\left[\frac{(2L)(2L-2)}{(2L-1)}\right]^{\frac{1}{2}}
$$

$$
\times \left[\sum_{j=-3}^{3}(R_3P_1)_{NL}^{j}I_{N'L-2;N+jL} + \sum_{j=-2}^{2}(L+1)(R_2)_{NL}^{j}I_{N'L-2;N+jL}\right]. \tag{D2}
$$

[1] T. Kazimierczuk, D. Fröhlich, S. Scheel, H. Stolz, and M. Bayer, Nature (London) **514**, 343 (2014).

[2] M. Aßmann, J. Thewes, D. Fröhlich, and M. Bayer, Nat. Mater. **15**, 741 (2016).

[3] F. Schweiner, J. Main, and G. Wunner, Phys. Rev. B **93**, 085203 (2016).

[4] P. Grünwald, M. Aßmann, J. Heckötter, D. Fröhlich, M. Bayer, H. Stolz, and S. Scheel, Phys. Rev. Lett. **117**, 133003 (2016).

[5] M. Feldmaier, J. Main, F. Schweiner, H. Cartarius, and G. Wunner, J. Phys. B **49**, 144002 (2016).

[6] J. Thewes, J. Heckötter, T. Kazimierczuk, M. Aßmann, D. Fröhlich, M. Bayer, M. A. Semina, and M. M. Glazov, Phys. Rev. Lett. **115**, 027402 (2015), and Supplemental Material.

[7] F. Schöne, S. O. Krüger, P. Grünwald, H. Stolz, S. Scheel, M. Aßmann, J. Heckötter, J. Thewes, D. Fröhlich, and M. Bayer, Phys. Rev. B **93**, 075203 (2016).

[8] F. Schweiner, J. Main, M. Feldmaier, G. Wunner, and Ch. Uihlein, Phys. Rev. B **93**, 195203 (2016).

[9] J. Heckötter, M. Freitag, D. Fröhlich, M. Aßmann, M. Bayer, M. A. Semina, and M. M. Glazov, arXiv:1610.05001.

[10] S. Zielińska-Raczyńska, D. Ziemkiewicz, and G. Czajkowski, arXiv:1610.00131.

[11] F. Schweiner, J. Main, G. Wunner, and Ch. Uihlein, Phys. Rev. B **94**, 115201 (2016).

[12] F. Schweiner, J. Main, and G. Wunner, arXiv:1609.04278 [Phys. Rev. Lett. (to be published)].

[13] S. Zielińska-Raczyńska, G. Czajkowski, and D. Ziemkiewicz, Phys. Rev. B **93**, 075206 (2016).

[14] S. Zielińska-Raczyńska, D. Ziemkiewicz, and G. Czajkowski, Phys. Rev. B **94**, 045205 (2016).

[15] G. Wannier, Phys. Rev. **52**, 191 (1937).

[16] R. J. Elliott, in *Polarons and Excitons*, edited by C. Kuper and G. Whitefield (Oliver and Boyd, Edinburgh, 1963), pp. 269–293.

[17] R. Knox, *Theory of Excitons*, Solid State Physics Supplement Vol. 5 (Academic, New York, 1963).

[18] R. Knox and D. Dexter, *Excitons* (Wiley, New York, 1981).

[19] A. Zhilich, J. Halpern, and B. Zakharchenya, Phys. Rev. **188**, 1294 (1969).

[20] V. Agekyan, Phys. Status Solidi A **43**, 11 (1977).

[21] S. L. Artyukhin, Ph.D. thesis, Rijksuniversiteit Groningen, 2012.

[22] D. Fishman, Ph.D. thesis, Rijksuniversiteit Groningen, 2008.

[23] J. Luttinger, Phys. Rev. **102**, 1030 (1956).

[24] Ch. Uihlein, D. Fröhlich, and R. Kenklies, Phys. Rev. B **23**, 2731 (1981).

[25] N. O. Lipari and M. Altarelli, Phys. Rev. B **15**, 4883 (1977).

[26] G. M. Kavoulakis, Y.-C. Chang, and G. Baym, Phys. Rev. B **55**, 7593 (1997).

[27] P. Schmelcher and L. S. Cederbaum, Z. Phys. D **24**, 311 (1992).

[28] P. Schmelcher and L. S. Cederbaum, Phys. Rev. A **47**, 2634 (1993).

[29] M. Altarelli and N. O. Lipari, Phys. Rev. B **7**, 3798 (1973).

[30] M. Altarelli and N. O. Lipari, Phys. Rev. B **9**, 1733 (1974).

[31] Y. Chen, B. Gil, H. Mathieu, and J. P. Lascaray, Phys. Rev. B **36**, 1510 (1987).

[32] J. Broeckx, Phys. Rev. B **43**, 9643 (1991).

[33] K. Suzuki and J. C. Hensel, Phys. Rev. B **9**, 4184 (1974).

[34] J. Hodby, T. Jenkins, C. Schwab, H. Tamura, and D. Trivich, J. Phys. C **9**, 1429 (1976).

[35] *Landolt-Börnstein*, edited by O. Madelung and U. Rössler, New Series, Group III, Vols. 17a to 17i, 22a and 22b, and 41, Pts. A to D (Springer, Berlin, 1982–2001).

[36] A. Edmonds, *Angular Momentum in Quantum Mechanics* (Princeton University Press, Princeton, NJ, 1960).

[37] A. Baldereschi and N. O. Lipari, Phys. Rev. B **8**, 2697 (1973).

[38] M. A. Caprio, P. Maris, and J. P. Vary, Phys. Rev. C **86**, 034312 (2012).

[39] E. Anderson, Z. Bai, C. Bischof, S. Blackford, J. Demmel, J. Dongarra, J. D. Croz, A. Greenbaum, S. Hammarling, A. McKenney *et al.*, *LAPACK Users' Guide*, 3rd ed. (Society for Industrial and Applied Mathematics, Philadelphia, PA, 1999).

[40] A. Abragam and B. Bleaney, *Electron Paramagnetic Resonance of Transition Ions* (Clarendon Press, Oxford, 1970).

[41] G. Koster, J. Dimmock, R. Wheeler, and H. Statz, *Properties of the Thirty-Two Point Groups* (M.I.T. Press, Cambridge, MA, 1963).

[42] O. Madelung, *Festkörpertheorie* (Springer, Berlin, 1972).

[43] *Polarons and Excitons*, edited by C. Kuper and G. Whitefield (Oliver and Boyd, Edinburgh, 1963).

[44] R. J. Elliott, T. P. McLean, and G. G. MacFarlane, Proc. Phys. Soc. **72**, 553 (1958).

[45] J. Fuchs, J. Main, H. Cartarius, and G. Wunner, J. Phys. A: Math. Theor. **47**, 125304 (2014).

[46] J. Main, P. A. Dando, Dž. Belkić, and H. S. Taylor, J. Phys. A: Math. Gen. **33**, 1247 (2000).